

EFFECT OF FORGING SURFACE ON FATIGUE BEHAVIOIR OF STEELS: A LITERATURE REVIEW

**SEAN MCKELVEY, GRADUATE RESEARCH ASSISTANT
AND**

ALI FATEMI, PROFESSOR

**THE UNIVERSITY OF TOLEDO
TOLEDO, OHIO**

Abstract

This paper presents a literature review on the surface finish effect on fatigue behavior of steel forgings. The effect of decarburization and surface roughness are discussed as they are often present in the as-forged surface. A description of roughness parameters and their accuracy in characterizing fatigue behavior is given. Some fatigue limit prediction models which use both fracture mechanics-based and notched-based approaches to evaluate the effects of surface roughness are then discussed. Since forged parts are commonly heat treated and shot cleaned, the effects of such treatments on fatigue behavior are also discussed.

1. Introduction

Forging is a commonly used manufacturing method. Vehicles are made of up to 25% forged components [1]. Most forgings are hot forged due to the fact that it allows for a more complex geometry than cold or warm forging. Hot forging is done at a temperature which allows recrystallization of the material being forged, typically around 1200°C for steels. When hot forging, the material can be heated up by use of gas furnace or induction heating. Induction heating is where electrical currents are used to heat up the material, and only the material, unlike gas furnace heating [2]. Induction heating heats the material more rapidly and uniformly. Gas furnace can produce more scale formation, oxidation, decarburization and grain coarsening [2].

Closed-die forging is done by placing a heated billet in between an upper and lower die and then bringing the upper and lower dies together. The heated material then fills the cavity in the die. In many cases excess material is allowed to protrude from a narrow gap between the upper and lower dies creating the flash. It is possible to produce closed-die forgings without flash; however this is a much more controlled, therefore more costly process and may not be necessary for most applications. Open-die forging is a similar process involving upper and lower dies. However, the dies are typically flat or have a simple contour. Open-die forgings also require larger tolerances compared to closed-die forgings and require more machining for close tolerances [3].

Although significant improvements to the steel making and forging processes have been made, the correction factors used in fatigue design for the as-forged surface condition are still based on data published in the 1930's and 1940's [4-6]. This results in an over engineered design of many mechanical parts, which is accompanied by an increase in production cost [7]. This paper reviews previous studies on the effects of surface condition, most importantly the as-forged surface condition, on the fatigue behavior of steels. It includes a discussion of the effect of inclusions and grain flow in forged steel on the fatigue behavior. The effects of decarburization, surface roughness, and shot blasting on fatigue behavior are presented. There is also a discussion of surface roughness parameters used to quantify surface roughness. Hardness effects on fatigue behavior of steels are also presented. This is followed by a discussion of crack growth behavior in steels with decarburization and surface roughness defects.

2. Effect of Inclusions and Grain Flow in Forged Steel on Fatigue Behavior

In a study by Collins and Michal [8] tension-tension fatigue tests ($R = 0.1$) were performed on forged specimens made of AISI 4140 steel in order to determine the effects of changes in shape and distribution of MnS inclusions. Three types of AISI 4140 steel were used, IGS/HS, IGS, and IGS/SC, each with a different composition. The specimens were machined from a forged block of material in both longitudinal and transverse directions. The specimens were then quenched and tempered to a hardness of 38 HRC with a tempered martensite microstructure. Finally, they were polished to a 0.25 μm surface finish. It should be noted that the specimens had compressive residual stresses at the surface around 357 MPa resulting from machining [8]. During the forging process, it is possible for the inclusions to be reoriented following flow lines. It is also possible for the inclusions to deform more than the material surrounding it during forging. They describe a method of controlling the shape of an inclusion, which has been shown to improve the fatigue life. Different chemicals and thermal treatments can be used. Adding calcium can harden the inclusions to prevent deformation during working. Figure 1 shows the shape change of MnS inclusions and Ca treated MnS inclusions. It can be seen that the treated inclusions experienced little change in shape. The results from fatigue testing showed that forging improved the fatigue behavior of the base material. The Ca treatment was shown to improve fatigue behavior by preventing the MnS inclusions from fracturing during forging. In addition, the grain flow and inclusion redistribution resulting from forging enhanced the mechanical properties of the base material.

Chastel et al [9] performed an analysis of the impact of forging on fatigue of steels. Their study involved a finite element model for analyzing the forging process. This model considers grain flow and anisotropy. Figure 2 shows the grain flow of a steel part. This grain flow can also lead to grain fragmentation and deformation of inclusions. Ductile inclusions can stretch. Hard inclusions are realigned. This results in anisotropic fatigue properties. Once the anisotropic mechanical properties are determined the authors suggest using the Murakami model, which predicts fatigue limit for specimens with defects and inclusions. The Murakami equation treats defects and inclusions as

cracks. The following equation is for determining the stress intensity factor at the tip of a surface defect or inclusion:

$$\Delta K = 0.65 \Delta \sigma \sqrt{\pi \sqrt{area}} \quad (1)$$

The \sqrt{area} parameter is defined as the defect area projected onto the plane perpendicular to the applied stress (see Figure 3). The following equation relates the threshold stress intensity factor range, ΔK_{th} , to the defect size:

$$\Delta K_{th} = 3(10)^{-3} (HV + 120)(\sqrt{area})^{1/3} \left[0.5 - \frac{R}{2} \right]^{0.226 + HV(10)^{-4}} \quad (2)$$

In this equation R is the stress ratio and HV is the Vickers hardness. When Eqns. 1 and 2 are combined, the result is:

$$\sigma_w = 1.43 \frac{HV + 120}{\sqrt{area}^{1/6}} \left[0.5 - \frac{R}{2} \right]^{0.226 + HV(10)^{-4}} \quad (3)$$

where σ_w is the fatigue limit (at 10^7 cycles). It should be noted that Eqn. 3 is for surface defects. For internal defects the constant in Eqn. 3 of 1.43 is changed to 1.56. The projected area of the inclusion perpendicular to the normal stress is used to characterize the anisotropic effects of the deformed inclusion.

3. Surface Finish

It is widely recognized that surface finish has a significant effect on fatigue behavior. Forging is usually accompanied by considerable surface roughness, surface decarburization and scale defects. In general, fatigue life decreases as surface roughness increases, particularly in the high cycle fatigue (HCF) region. Surface roughness has less of an effect in the low cycle fatigue (LCF) region. Decarburization results from forging process as well as heat treatment. It can be described as a reduction of carbon starting from the surface. Decarburization results in a reduction of hardness in the decarburized area. Surface cleaning treatments such as sand blasting decrease the effect of the as-forged surface finish by removing scale defects, as well as some of the decarburized layer, and to some extent inducing compressive residual stresses at the surface.

3.1 Decarburization

Hankins and Becker [5] tested forged specimens of different hardness under cantilever type rotating bending on four types of forged steels, as listed in Table 1. The as-forged surface finish specimens had an hourglass shape with a 0.3125 inch (7.94

mm) test section diameter. Machined and polished specimens had an hourglass shape with a 0.25 inch (6.35 mm) diameter. Half of the specimens were tested in the as-forged condition. It should be noted that the flash had been trimmed before testing. The other half had the as-forged surface removed prior to testing. A metallurgical analysis of the test specimens showed that the hardness of the decarburized surface was lower than the hardness of the inner material (see Table 1). There is less of a difference between surface and core hardness as specimen hardness decreases. The specimens with the largest difference between surface and interior hardness had the largest difference in endurance limit between the polished and as-forged surface conditions (see Table 2 and Figure 4). The authors state that decarburization is the main cause of reduced fatigue life for specimens of the as-forged surface condition.

Hankins et al [6] then performed further experiments on the effects of surface conditions on fatigue resistance of steels. In their study high tensile strength forgings were subjected to rotating bending fatigue. The fatigue specimens had the same dimensions as in their previous study [5]. The high tensile strength as-forged specimen had a very low endurance limit when compared to the machined and polished condition (see Table 3 and Figure 4). Normally the endurance limit of a polished specimen is around half of the ultimate tensile strength. However, in Table 3, it can be seen that the endurance limit of the polished specimens is only around 40% of the tensile strength. As a result, the author decided to subject the machined specimens to a better polishing procedure, which resulted in a significant improvement in endurance limit (683 MPa increased to 896 MPa). The authors suggest that the surface irregularities may have more of an effect on fatigue strength than the surface decarburization for high tensile strength forgings.

In a paper by Noll and Lipson [4], as-forged specimens of different hardness levels were investigated. It was found that the surface hardness was much lower than the hardness of the inner material for the forged specimens due to the decarburization, similar to results from Hankins et al. Figure 5 shows plots of the Brinell hardness versus distance from the surface for specimens of four hardness levels. Figure 6 shows magnified photographs of the specimens cross-section showing the decarburized layer. It should be noted that the pictures in Figure 6 correspond to the plots in Figure 5. The lighter colored area shown in the pictures represents the decarburized section. It can be seen in Figure 5 that the surface hardness was significantly lower than the interior hardness. This difference in hardness is one explanation for decreased life in the HCF region for forged specimens, since higher hardness (higher strength) is a desired property for long fatigue life. As previously mentioned, controlled forging can result in less decarburization and increased endurance limit, as seen in Figure 7, which shows a plot of endurance limit versus tensile strength for as-forged specimens. There are two curves in this figure, with the upper curve representing a controlled forging process and the lower curve representing a less controlled (standard large scale manufacturing) forging process [10]. The controlled forging process results in decarburization depths less than 0.13 mm, compared to depths as deep as 0.89 mm for the less controlled process [10]. In addition, the controlled forging process results in less surface irregularities than the standard large scale forging process.

Gildersleeve [11] investigated the relationship between decarburization and fatigue strength of a low alloy steel (605 M36). Rotating bending tests were used to determine the fatigue behavior. The specimens had decarburized layers up to 1 mm in depth. The results showed that the fatigue limit was mostly independent of the depth of decarburization (see Table 4). The author also examined surface carbon concentration and found the fatigue limit to be linearly dependent upon the carbon concentration at the surface.

Adamaszek and Broz [12] investigated the effects of decarburization on hardness changes in carbon steels caused by high temperature surface oxidation. The decarburization they studied resulted from annealing. They state that the decarburization causes the grains near the surface to grow. In addition to grain growth, there is formation of surface scales, which are solid, firm and porous. The authors explain that during the decarburization process oxygen penetrates the surface through cavities, pores and cracks. This oxygen reacts with the different chemicals (elements) in the metal causing the decarburization. The decarburization is worse for metals with higher Fe concentration. The authors also state that there are hardness changes due to the decarburized layers resulting in lower fatigue resistance.

3.2 Roughness measurements and parameters

Before determining how surface roughness affects fatigue life, it is necessary to measure and define surface roughness. The most common method of measuring surface roughness is the mechanical profiler. It works by dragging a stylus (probe) across the surface [13, 14]. As the stylus is drawn slowly across the surface, it moves up and down with the contours of the surface. This motion is then recorded. However, this instrument is limited by the radius of the stylus tip. If the radius is too large it may not be able to penetrate the finer cracks or scratches, resulting in an incorrect surface roughness measurement. It is also a possibility that the surface could be damaged by the stylus. A non-destructive method of measuring surface roughness is the laser speckle contrast method [13]. In this method a helium-neon light is pointed at the surface at various angles. As this light hits the surface it is reflected creating a speckle. It was found [13] that there is a linear relationship between the surface roughness and the speckle contrast of an illuminated surface up to a certain roughness ($0.1 \mu\text{m } R_a$).

Once the surface topography is recorded it is necessary to define it. Gadelmawla et al [15] describe 59 different parameters for describing surface roughness. The authors state that the arithmetic average height parameter (R_a), also known as the center line average (CLA), is the most widely used parameter. This parameter is the average deviation from the mean line over a sampling length (see Figure 8(a)). This is shown mathematically below:

$$R_a = \frac{1}{l} \int_0^l |y(x)| dx \quad (4)$$

While R_a is easy to define, it does not describe wavelength and is not sensitive to small changes in roughness profile. It should be noted that when reporting the value of R_a it is

necessary to also report the cutoff length, which is the length that the roughness is averaged over. R_q or RMS is the root mean square roughness, which is the standard deviation of the distribution of surface heights, and is another common parameter. R_q is more sensitive to a large deviation from the mean line than R_a . This parameter is expressed mathematically as:

$$R_q = \sqrt{\frac{1}{l} \int_0^l \{y(x)\}^2 dx} \quad (5)$$

The parameter R_z , known as the ten-point height, is defined as the difference in height between the average of the five highest peaks and the five lowest valleys (see Figure 8(b)). It should be noted that R_a is not as sensitive to occasional peaks and valleys as R_z . R_z is defined mathematically by:

$$R_{z(DIN)} = \frac{1}{n} \left(\sum_{i=1}^n p_i + \sum_{i=1}^n v_i \right) \quad (6)$$

The maximum height of profile parameter, R_t , is most sensitive to large peaks and valleys. It is defined as the distance measured between the highest peak, R_p , and the lowest valley, R_v , (see Figure 8(c)). It is defined mathematically by:

$$R_t = R_p + R_v \quad (7)$$

In Figure 8(c), R_v is equal to R_{v4} and R_p is equal to R_{p3} . Therefore, R_t is equal to $R_{p3} + R_{v4}$. In Figure 8(c), R_y , not to be confused with R_t , is the largest peak to valley height (i.e. $R_{p3} + R_{v3}$).

Mean spacing between peaks, S_m , is another parameter used to characterize surface roughness. It is defined as the mean spacing between profile peaks at the mean line (see Figure 8(d)) and is defined mathematically as:

$$S_m = \frac{1}{N} \sum_{i=1}^n S_i \quad (8)$$

There are many more parameters used to quantify surface roughness. Each parameter is designed to be more sensitive to different variations in roughness such as height and depth of roughness, frequency of roughness and distance between peaks.

Novovic et al [16] performed a literature review on the effect of machined surface topography and integrity on fatigue life and examined different roughness parameters. They examined surface roughness parameters and concluded that R_a is the most commonly used parameter in describing fatigue behavior. However, they found that there is typically a 20% scatter in fatigue results for specimens of the same R_a value. The authors suggest that R_t and R_z are better to use in determining fatigue performance than R_a , because these parameters represent the worst defects in the surface.

3.3 As-forged surface condition

As stated earlier, most of the available data for the effect of as-forged surface condition on fatigue are old and very conservative. The paper entitled “Allowable Working Stresses” by Noll and Lipson [4] is one of the main sources of data used to develop the endurance limit modification factors for the as-forged surface condition, which are still used in fatigue design and analysis. The authors investigated the relationship between endurance limit (defined at 10^7 cycles to failure) and surface condition (ground, machined, hot-rolled, and forged). The forged surface condition is described as having large surface irregularities, including oxide, scale defects, as well as total surface decarburization and is regarded as the worse of the above mentioned surface conditions. They grouped fatigue data on steels with hardness ranging from 160 HB to 555 HB from previous studies by other authors into the above categories. Some of the data for the as-forged surface condition are from data published by Hankins et al [5, 6]. However, most of the data for the as-forged surface condition were obtained from fabricated parts tested at the Chrysler Laboratories. The actual test data and experimental details performed at Chrysler Laboratories, from which the data were derived, are not included in [4]. From this data, Noll and Lipson developed several figures of allowable stress versus mean stress for each type of specimen (see Figure 9 for an example). Data from the 1945 version of the SAE Handbook were used by Noll and Lipson to define the relationship between tensile strength and hardness (see Figure 10), which is a mostly linear relationship. Noll and Lipson used the most conservative values from Figure 10 in their analysis. In addition, they developed a figure plotting endurance limit versus tensile strength (see Figure 11) for the four surface conditions investigated. The data used to develop Figure 11 is listed in Table 5. It can be seen in Figure 11 that the as-forged surface condition results in the lowest endurance limit for a given tensile strength of the four surface conditions described in [4]. It should be noted that controlled forging conditions can produce surface finish quality similar to hot-rolled surfaces [10].

In a discussion of the paper “Allowable Working Stresses,” Lessells compares endurance limit data on as-forged and ground and polished surface conditions from Noll and Lipson to data from Hankins et al [5, 6]. Lessells found the data from Noll and Lipson to be much more conservative than the data from Hankins et al. Noll and Lipson in their reply state that the discrepancies are due to modification of data for size effect, reducing Hankins endurance limit data by 15%. Noll and Lipson explain that there is more of a difference between data for forged surface than for the ground and polished surface due to the broad definition of the forged surface condition.

3.4 Effect of surface roughness on fatigue behavior

Fluck [17] studied the influence of surface roughness on fatigue life and scatter of test results of two steels. The steels used for the cantilever rotating bending tests were a quenched and tempered SAE 3130 steel (30 HRC) and an annealed SAE 1035 steel (69 HRB). The specimens, which were machined from 12.7 mm rolled bars, were grouped into six categories of surface roughness, lathe-formed, partly hand-polished,

hand-polished, ground, ground and polished, and superfinished. The surface roughness measurements were made with a Brush surface analyzer. This instrument indicated the root mean square of the surface roughness. Figure 12 shows a plot of the $RMS (R_q)$ surface roughness versus median fatigue life. The results show that the ground and polished specimens, which represent the smoothest surface, always experienced the longest life and the lathe-formed specimens, which represent the roughest surface, experienced the shortest life.

Figure 13 shows the scatter of these results. It can be seen in Figure 13 that there is generally more scatter for a given polishing condition at longer life for both of the materials used. The author concluded that fatigue life can be significantly increased by reducing the size of circumferential scratches. Specimens polished to roughness below six microinches experienced a large increase in fatigue life. In a discussion of this paper, Lessells points out that the author did not consider surface residual stresses and surface hardening through cold work and martensite formation that could have been introduced by the polishing procedures. As a result, according to Lessells, surface roughness is not the only cause for the differences in fatigue life data reported by Fluck.

Sibel and Gaier [18] investigated the influence of surface roughness on fatigue strength of steels and non-ferrous alloys [18]. Axial and reverse bending fatigue tests were performed on several types of steels (medium carbon, Cr-Mo, spring steel, and stainless) as well as brass and some aluminum alloys. Roughness was applied to the specimen surface by polishing, grinding and turning. The specimens had an hour glass shape with 8.4 mm and 7.5 mm minimum diameters for the axial and bending specimens, respectively. The roughness parameter used was R_v , the maximum depth of groove, with values ranging from 1 to 50 microns. There was a similar decrease in fatigue strength, for both axial and reverse bending fatigue tests, as surface roughness increased.

3.5 Fatigue limit evaluation for surface finish effect

Murakami and Endo [19] performed an extensive literature review on the effects of defects, inclusions and inhomogeneities on fatigue strength and the existing models. The authors classify the different approaches into three categories: empirical models, models based on fatigue notch factor approach, and fracture mechanics models. Many of them can be used to determine behavior of specimens with scratches, cracks or notches.

As presented earlier, Murakami et al developed an equation (Eqn. 3) for prediction of the fatigue limit for specimens with small defects and inclusions [19]. Although this equation was developed for specimens with small defects and inclusions, they have shown it to be applicable to surface roughness conditions by performing rotating bending fatigue testing on a medium carbon JIS S45C steel [20, 21]. The specimens were machined after heat treatment or annealing (see Figure 14 for specimen configuration and dimensions). After machining, artificial roughness in the form of notches of various depth and pitch was applied to the specimens by use of a lathe. The depth of the artificial roughness was considered random because of build up on the cutting tool, but the pitch between notches was considered constant (see Figure

15 for magnified views of the different types of artificial surface roughness applied). There were also some electro-polished specimens. Some of the electro-polished specimens had a single notch applied to them after polishing. Roughness was measured by use of a mechanical profiler. Figure 16 shows a plot of the stress-life data. All fatigue failures occurred at the root of an artificially induced notch. The fatigue strength decreased as the depth of the notch increased. It was shown that the specimens with a single notch experienced fatigue strength that was about 30% lower than that of specimens with multiple notches. This is because interference between notches reduces the fatigue notch effect. As a result the authors determined that the pitch between notches must be considered, which is not considered in the \sqrt{area} parameter.

In order for Eqn. 3 to be used to evaluate surface roughness, Murakami et al developed an equivalent defect size for surface roughness $\sqrt{area_R}$ to replace \sqrt{area} , which accounted for both depth and pitch. They assumed that periodic roughness notches are equivalent to periodic cracks. It should be noted that this problem was evaluated as a crack problem and not a notch problem. They derived the following equations:

$$\frac{\sqrt{area_R}}{2b} \cong 2.97(a/2b) - 3.51(a/2b)^2 - 9.47(a/2b)^3 \quad \text{For } a/2b < 0.195 \quad (9)$$

$$\frac{\sqrt{area_R}}{2b} \cong 0.38 \quad \text{For } 3 > a/2b > 0.195 \quad (10)$$

where a is the crack depth and $2b$ is the distance between the two cracks. Figure 17 shows a plot of $\sqrt{area_R}/2b$ versus $a/2b$. This figure includes superimposed data points calculated from experimental data. When considering value of depth, a , the authors chose to use the maximum height parameter R_y . The following equation was used to calculate the fatigue limit for the electro-polished specimens (without notch) and the artificially roughened specimens, respectively:

$$\sigma_w = 1.6HV \quad (HV \leq 400) \quad \text{For polished surface condition} \quad (11)$$

$$\sigma_w = \frac{1.43(HV + 120)[(1 - R)/2]^\alpha}{(\sqrt{area_R})^{\frac{1}{6}}} \quad \text{For rough surface condition} \quad (12)$$

Table 6 displays the $\sqrt{area_R}$ values for each type of artificial surface roughness. Table 7 shows the experimental and calculated values of fatigue limit along with the hardness values and the $\sqrt{area_R}$ parameter. Materials 100A and 150QT listed in Tables 6 and 7 have similar crack depth, but different pitch (100 μm , 150 μm and 200 μm). The numbers in the specimen ID listed in Tables 6 and 7 refer to the pitch. It can be seen

that the decreased pitch distance results in a lower value of $\sqrt{area_R}$. This lower value of $\sqrt{area_R}$ would result in a larger value of σ_w , which is in agreement with experimental data. Figure 18 shows a plot of the experimental life versus the predicted life using Eqns. 11 and 12, showing an error less than 10% in predicting fatigue limit for most specimens.

Shareef and Hasselbusch [7] investigated endurance limit modifying factors for hardened machined surfaces. They state that existing surface finish modification factors, derived from “Allowable Working Stresses,” are limited to hardness up to 33 HRC, and when this factor is extrapolated to higher hardnesses it produces overly conservative values. The authors performed fatigue tests on specimens made from SAE 4140 steel with a machined surface and hardness ranging between 50 and 55 HRC. The average hardness of the specimens tested was 53.4 HRC. The roughness was defined by the R_a parameter. The specimens had an average roughness of 3.51 μm . The specimens also had surface compressive residual stresses with an average value of -331 MPa. Figure 19 shows the specimen geometry as well as the test set up used. The shafts were subjected to three-point bending while strain was monitored using gages. They used three different stress equivalency methods to calculate the surface finish correction factor, k_a :

$$\left(\frac{\sigma_a}{S_e}\right)_{machined} = k_a \left(\frac{\sigma_a}{S_e}\right)_{polished} \quad (13)$$

$$\left(\frac{\Delta\epsilon}{2}\right) = \frac{k_a(\sigma_f' - \sigma_0)}{E} (2N_f)^b + \epsilon_f' (2N_f)^c \quad (14)$$

$$\left(\sigma_{max} \frac{\Delta\epsilon}{2}\right) = \frac{(k_a \sigma_f')^2}{E} (2N_f)^{2b} + k_a \sigma_f' \epsilon_f' (2N_f)^{b+c} \quad (15)$$

They solved for k_a and found that the SWT relationship (Eqn. 15) resulted in the best predictions. Table 8 shows the correction factors calculated using Eqns. 13-15 for 10^4 and 10^6 cycles to failure. It should be noted that in Eqns. 14 and 15, k_a was applied to only the elastic portion of the curve. Figure 20 shows that Eqns. 14 and 15 result in a decreased effect of surface roughness with a decrease in fatigue life, but Eqn. 13 shows no difference between LCF and HCF. Existing data, derived from “Allowable Working Stresses,” gives an endurance limit modification factor of $k_a = 0.44$ for machined specimens at 53.4 HRC. Shareef and Hasselbusch state that the use of their most conservative modification factor $k_a = 0.75$, derived from Eqn. 13, would result in cost and weight savings up to 50%. This is an example of how conservative the data published by Noll and Lipson are.

Arola and Williams [22] investigated the effects of surface texture on a high strength low alloy steel. In their investigation, surface roughness parameters were used

to calculate an effective stress concentration factor, which was then used to determine an effective fatigue notch factor. The effective stress concentration factor based on roughness parameters was defined as:

$$\bar{K}_t = 1 + n \left(\frac{R_a}{\bar{\rho}} \right) \left(\frac{R_y}{R_z} \right) \quad (16)$$

where R_a is the average roughness, R_y is the peak to valley height, R_z is the 10-point roughness, and $\bar{\rho}$ is the average radius determined from the dominant profile valleys (see Figure 21 for definition of $\bar{\rho}$). The value of n in Eqn. 16 is equal to two for uniform tension loads and equal to one for shear loads. Equation 16 can then be substituted into Eqn. 17 below to calculate an effective fatigue notch factor, as:

$$\bar{K}_f = 1 + q(\bar{K}_t - 1) \quad (17)$$

In Eqn. 17, q is defined as the notch sensitivity and is given by:

$$q = \frac{1}{\left(1 + \gamma / \bar{\rho} \right)} \quad (18)$$

where γ for steels is define by:

$$\gamma = 0.025 \left(\frac{2070 \text{ MPa}}{\sigma_u} \right)^{1.8} \quad (19)$$

In Eqn. 19, σ_u is the ultimate tensile strength in MPa and γ is in units of mm. Figure 22 shows a plot of fatigue stress concentration factor versus average surface roughness. This plot superimposes calculated values along with experimental values. It can be seen that the proposed equation for stress concentration factor is in good agreement with the experimental data.

Stephens et al [23] state that the fatigue notch factor can be applied to the modified Goodman equation as follows:

$$\frac{S_a}{\left(S_f / K_f \right)} + \frac{S_m}{S_u} = 1 \quad (20)$$

where S_a is the net section alternating stress, S_f is the fully-reversed fatigue strength for a smooth unnotched specimen, S_m is the mean stress, and S_u is the ultimate tensile strength. Therefore, it is then possible to apply the effective fatigue notch factor

calculated from Eqn. 17 to the modified Goodman equation to account for mean or residual stresses, stress concentration, and surface finish effects.

There are many textbooks and handbooks that describe how surface finish affects fatigue life. The methods of evaluating the as-forged surface condition presented in them give conservative values. Mechanical design and fatigue textbooks generally provide an equation for determining the endurance limit for the surface finish condition (for example in [24]), as well as other factors, by use of correction factors, given by:

$$S_e = k_a k_b k_c k_d k_e k_f S'_e \quad (21)$$

In this equation k_a is the surface modification factor, k_b is the size modification factor, k_c is the load modification factor, k_d is the temperature modification factor, k_e is the reliability factor, k_f is the miscellaneous-effects modification factor, and S'_e is the endurance limit from rotating bending fatigue tests performed on smooth polished specimens. The surface modification factor is defined as:

$$k_a = a S_{ut}^b \quad (22)$$

In this equation S_{ut} is the ultimate strength and a and b are constants found in Table 9. Table 9 provides values of a and b for the ground, machined, hot-rolled and as-forged surface conditions. These values are derived from the paper “Allowable Working Stresses [4]” discussed earlier. Figure 23 shows a plot of surface finish factor versus tensile strength presented in many mechanical design and fatigue books [such as 23-32] which is derived from the data presented in Figure 11. The authors of “Allowable Working Stresses” determined endurance limit at 10^7 cycles when developing Figure 11 [4]. However, it is suggested by Noll and Lipson [10] that steels reach the endurance limit value around 10^6 cycles, as seen in Figure 24, which shows a plot of stress versus cycles to failure for as-forged surface finish specimens of two hardness levels [10]. It is mentioned that the surface finish factor has an increasing effect with an increase in tensile strength or hardness, which can be seen in Figure 23. In addition, the surface finish effect is generally thought to be negligible for specimens subjected to less than a thousand cycles due to a high degree of plastic deformation. Figure 25 shows an example of S-N behavior for specimens having machined and polished surface and as-forged surface conditions. It can be seen that the curves intersect at 10^3 cycles.

The load factor, k_c in Eqn. 21, which accounts for the type of loading the specimen is subjected to is given by [24]:

$$k_c = \begin{cases} 1 & \text{rotating bending} \\ 0.85 & \text{axial loading} \\ 0.577 \rightarrow 0.59 & \text{torsion} \end{cases} \quad (23)$$

The correction factor for rotating bending is one because S'_e is the endurance limit under rotating bending loading, therefore no correction is needed.

Size effect modification factor, k_b , corrects for diameters larger than about 7 mm, since a standard diameter of a test specimen is about 7 mm [24]. For specimens between 12 mm and 25 mm diameter, there is around a 15% reduction in fatigue limit under rotating bending loading. For specimens larger than 50 mm in diameter, the fatigue strength can be 25% lower than the standard specimen's fatigue strength under rotating bending loading. The size factor is given mathematically by:

$$k_b = \begin{cases} (d/0.762)^{-0.107} & 2.79 \leq d \leq 51 \text{ mm} \\ 1.51d^{-0.157} & 51 < d \leq 254 \text{ mm} \end{cases} \quad (24)$$

For nonrotating bending the size effect is less significant. This is because there is a lower volume of material subjected to maximum stresses under nonrotating bending. The lower volume of material is accounted for by using an effective diameter in Eqn. 24, given by:

$$d_e = 0.37 d \quad (25)$$

The difference between rotating and nonrotating bending fatigue strength is regarded as typically less than 5% for commercial materials [32].

4. Sand Blasting and Shot Cleaning

Sand blasting is a process in which sand is shot, by air, at the surface of a component for the purpose of cleaning the surface. It is an effective method of removing the scale left from forging and heat treating operations. There are other methods of treating the surface such as shot peening, nitriding and other chemical processes, but these surface enhancement processes are outside the scope of this review. The sand blasting process induces compressive residual stresses at the surface as well as increased surface roughness. Sand blasting typically produces compressive layers between 25 and 75 μm deep compared to compressive layers between 100 and 300 μm resulting from the shot-peening process [16]. The depths of the compressive layers for sand blasting mentioned are, however, for a well-controlled sand blasting process in which the compressive stresses are intentional. This is not to be confused with a sand blasting process whose intentions are to clean the surface, which also typically leaves unintentional beneficial compressive residual stresses. Typically the sand blasting treatment for steels increases fatigue life in the HCF region due to the beneficial compressive residual stresses, but may decrease fatigue life in the LCF region due to reduced surface ductility.

Hanley and Dolan [33] conducted a literature review on surface finish and its effect on fatigue behavior. They refer to a study by Wiegand [34], which concluded that shot blasting increased the fatigue strength (at 10^7 cycles) of a smooth surface by 10

MPa as well as a roughened surface by 90 MPa. Wiegand also found that sand blasting decreased fatigue strength (at 10^7 cycles) of a polished surface by about 48 MPa. In a study by Manteuffel [35] sand blasting was shown to improve fatigue strength (at 10^7 cycles) of steel springs. Hanley and Dolan explained that the differences in fatigue data from [34] and [35] were due to the initial surface conditions, polished and unpolished. Zimmerli [36] subjected shot blasted springs to fatigue testing and found that fatigue strength (at 10^7 cycles) was improved by the shot blasting process. He also found that a smaller sized shot (0.4 mm diameter) improved long life fatigue behavior for a given maximum stress, compared to a larger shot (1.2 mm diameter). In addition, he found that light sand blasting following the shot blasting further increased fatigue life for a given maximum stress. However, neither the shot blasting (0.4 mm shot) nor shot blasting (0.4 mm shot)/sand blasting increased the fatigue strength at 10^7 cycles compared to the larger shot, it only increase fatigue life for a given stress level.

Farrahi et al [1] studied the influence of residual stress on the fatigue life of forged and shot blasted components. In their study hot forged round EN15R steel bars were subjected to uniaxial tension-compression fatigue tests. Specimens were forged by use of induction heat and cooled in room temperature air. The forged specimens had an hourglass shape with a minimum diameter of 8.2 mm. Some of the forged specimens were heat treated and/or sand blasted. The flash line had been trimmed prior to heat treatment and shot blasting. The sand blasting was done to clean the scale off the specimen as well as to induce compressive residual stresses. Results showed that sand blasting was beneficial in the HCF region due to compressive residual stresses (see Table 10). However, sand blasting was found to be detrimental in the LCF region due to relaxation of the compressive residual stress resulting from plastic deformation in the LCF region and reduced ductility due to plastically deformed surface. The sand blasting treatment increased scatter of test results in both LCF and HCF regions.

5. Heat Treatment and Hardness Effects

5.1 Heat treatment

Heat treatment of steels, which is done to control material properties, to a large extent is dependent on carbon content adding strength to the material [37-40]. Iron can take two crystallographic orientations, BCC and FCC, which can be seen in Figure 26. The iron changes from one atomic structure to another when it is heated to a certain temperature. The solubility of carbon is higher for the FCC orientation. By controlling the rates of heating and cooling of the material, properties of the material can be controlled. Slowly cooling the material allows the carbon to leave the metal. However rapid cooling traps the carbon in the material making it harder. It should be noted that this is a reversible process.

Quenching and tempering is a common heat treatment procedure. Table 11 lists a variety of other heat treatment procedures for steels along with their purpose. The idea behind quenching and tempering is to quench the material when it has reached the austenite phase (see Figure 27, a phase diagram plotting the temperature versus the carbon concentration). It can be quenched in different liquids such as water or oil. Once

quenched, the material rapidly cools and martensite forms. Figure 28 shows a plot of hardness of martensite versus carbon content, indicating the hardness increases with increasing carbon content. Following quenching, it is necessary to temper the material because the quenched material is brittle and contains internal stresses. The internal stresses are caused by expansion and contraction of the material during the heating and cooling process.

Tempering is done by reheating the material to various temperatures to obtain desired properties as well as relieve internal stresses [37-40]. Figure 29 shows a plot of tensile and yield strength versus the tempering temperature for an oil-quenched 4340 steel having a martensitic microstructure [40]. This figure shows that tempering at lower temperatures allows the material to maintain strength or hardness while relieving internal stresses. As tempering temperatures increase the ductility of the material increases but the strength or hardness decreases. Some side effects of quenching and tempering are cracking and decarburization. Cracking can be caused by quenching from too high of a temperature or by non-uniform heating and cooling. Decarburization is caused by an oxidizing atmosphere similar to decarburization resulting from the forging process, already discussed.

The Steel Heat Treatment Handbook [38] describes how undesirable distortion can occur during the heat treatment process. Material properties will affect thermal expansion of the material, which if not accounted for can cause residual stresses to form during quenching. The homogeneity of the material should be considered. Large variations of composition across the cross section of the material can cause unwanted residual stresses during heat treatment. The residual stresses induced by processes such as forging or hot rolling can be relieved during the heat up portion of the heat treatment process. However, when these stresses are released, it can cause the part to deform. There are also shape changes due to phase changes during heat treatment. There is about a 4% reduction in volume when iron transforms from the pearlite phase to the austenite phase. As a heat treated part cools, residual stresses can form, mostly due to phase changes. However, residual stresses can be minimized by slowing down the cooling rate.

5.2 Hardness effects on fatigue behavior

Hankins et al investigated the fatigue resistance of unmachined forged steels [5, 6]. Results of the monotonic tension testing show that as hardness increases so does the tensile strength. Their fatigue test results show that the harder the material the greater the difference in endurance limit between as-forged and polished specimens. This can be seen in Figure 4, which shows a plot of endurance limit (at 10^7 cycles) versus tensile strength for as-forged and polished materials tested in [5, 6]. The fatigue limit for the as-forged surface is up to 83% lower than the polished surface for the hardest material, but only 15% lower for the softest material tested (see Tables 2 and 3). It should be noted that the softest material was not quenched and tempered, which was not the case for the other materials. As mentioned in the section on decarburization (section 3.1), Hankins et al attribute decarburization to the decrease in endurance limit for the as-forged specimens of hardness below 308 HB. They also state that the surface

condition is of more importance to materials of higher hardness, as in the case of the two high strength steels tested (listed in Table 3).

In "Allowable Working Stresses," by Noll and Lipson [4], they grouped data from other investigators into different types of surface condition with different hardnesses ranging from 160 HB to 555 HB. It was shown that the surface condition had an increasing effect with increased hardness, which can be seen in Figure 11 in a plot of endurance limit versus tensile strength. This plot shows that there is little to no increase in endurance limit for a given tensile strength for the as-forged surface condition. Fluck [17] found similar results when investigating surface roughness effects on two steels, SAE 3130 (30 HRC) steel and an annealed SAE 1035 (69 HRB) steel. It was also shown by Noll and Lipson that a linear relationship exists between tensile strength and Brinell hardness (see Figure 10).

Landgraf [41] investigated cyclic deformation and fatigue behavior of hardened steels. SAE 1045 and SAE 4142 steels were used in their study. The specimens were machined and then heat treated to five different hardness levels ranging from 380 HB to 670 HB. Strain-controlled completely-reversed axial fatigue tests were performed. Step tests for cyclic deformation and monotonic tension tests were also performed. The results of monotonic testing showed a linear increase in true fracture strength with an increase in hardness up to 600 HB. After 600 HB, the true fracture strength began to decrease. Figure 30 shows superimposed plots of monotonic and cyclic stress-strain curves for the different hardnesses for the SAE 1045 and SAE 4142 steels. It can be seen that most specimens cyclically softened and the degree of cyclic softening decreases as hardness increases. However, at the two highest hardness levels for the SAE 4142 steel (670 HB and 560 HB) the material cyclically hardened. Figure 31 shows plots of stress amplitude versus plastic strain amplitude for the different types of specimens used. This figure shows very little effect on the cyclic strain hardening exponent with changes in hardness; however there is an increase in cyclic strength coefficient with an increase in hardness. Figure 32 shows plots of total strain amplitude versus reversals to failure for SAE 1045 steel at 700 HB, 600 HB, and 450 HB, as well as SAE 4142 steel at 670 HB, 560 HB, and 450 HB. Figure 33 shows plots of total strain amplitude versus hardness at different cycles to failure for SAE 1045 steel and SAE 4142 steel. It can be seen in these figures that softer materials show better fatigue resistance in the LCF region due to the increased ductility. In contrast, the harder materials show better fatigue resistance in the HCF region due to increased strength.

6. Crack Growth Behavior

6.1 Fracture mechanics

Stress-life and strain-life analysis do not distinguish between crack initiation and crack growth. Typically, for smooth unnotched fatigue specimens, most of the life is taken up by crack initiation. However, for parts having a rough surface, micro-cracks may exist prior to loading depending on the severity of the roughness. The majority of life for a part containing surface cracks will consist of crack growth. Fracture mechanics characterizes fatigue crack growth behavior by use of a stress intensity factor or the J-

integral. There are two types of fracture mechanics analysis, linear elastic fracture mechanics (LEFM) and elastic-plastic fracture mechanics (EPFM). The type of fracture mechanics analysis used is dependent upon crack-tip behavior. Although the nominal stress applied to a part may be elastic, the stress concentration resulting from the crack can cause significant plastic deformation at the crack tip. LEFM may be used when the plastic deformation at the crack tip is small, and this is the case in most fatigue problems. EPFM is used when there is significant plastic deformation at the crack tip [23].

A LEFM approach to modeling crack growth behavior under mode I (i.e. tensile mode or opening crack mode) which is most common in applications is applied by plotting crack growth rate, da/dN , versus stress intensity factor range, ΔK , in a log/log plot, where:

$$\Delta K = \Delta S \sqrt{\pi a} \alpha \quad (26)$$

In this equation, ΔS is the stress range (zero stress to maximum stress if the minimum stress is compressive), a is the crack length, and α is a geometry factor dependent upon crack geometry and loading mode. The change in crack length divided by the change in cycles (da/dN) is the rate at which the crack grows. Figure 34, which is for the linear Paris equation regime with crack growth rates higher than 10^{-8} m/cycle, shows crack growth rate versus stress intensity factor range for a wide range of martensitic steels having tensile strengths ranging from 730 MPa to 1290 MPa. The Paris equation is given by:

$$\frac{da}{dN} = A (\Delta K)^n \quad (27)$$

where A is the intercept at $\Delta K = 1$, and n is the slope. It can be seen in this figure that there is relatively little scatter for a type of steel having the same microstructure with data falling in between two narrow scatter bands. This suggests that the applied stress intensity factor range is the governing factor controlling crack growth behavior in steel and not material properties (i.e. yield strength, tensile strength and ductility) [42]. Use of the upper scatter band equation would result in conservative predictions of crack growth rates.

6.2 Fatigue crack growth

Arieli and Mukherjee [43] performed tension-tension cyclic tests on notched specimens in order to determine the effects of decarburization on fatigue life (see Figure 35 for specimen dimensions). The material used was a 4340 low alloy steel with an ultimate tensile strength of 965 MPa. They stated that residual tensile stresses may be present in the decarburized layer due to volumetric contraction of the low carbon area by the higher carbon content of the inner material. Test results showed that fatigue life improved in the LCF region for decarburized specimens compared to specimens without

decarburization. As the decarburization depth increased, so did the fatigue life for a given stress amplitude, as shown in Table 12, which lists fatigue life for various decarburization depths, were a_d indicated depth of decarburization. However, decarburization eliminated the possibility of run-out. This behavior is believed to be due to crack growth behavior of the decarburized layer [43]. The authors also noted that degree of fatigue life improvement was dependent upon the maximum applied stress and not the stress amplitude. The fatigue test results listed in Table 12 include the total fatigue life (N_t), the fatigue life for crack to grow through the decarburized layer (N_d), and fatigue life for crack to grow from the end of the decarburized layer to the critical length (N_b). Therefore, the total fatigue life was defined by:

$$N_t = N_d + N_b \quad (28)$$

$$N_d = \frac{(a_0)^{-0.5} - (a_d)^{-0.5}}{1.8(10^{-10})(\Delta\sigma\sqrt{\pi})^3} \quad (29)$$

$$N_b = \frac{(a_d)^{-0.125} - (a_{cr})^{-0.125}}{0.0825(10^{-8})(\Delta\sigma\sqrt{\pi})^{2.25}} \quad (30)$$

Values of a_0 and a_d are also listed in Table 12. It should be noted that Eqns. 29 and 30 were obtained by integrating the Paris equation.

Maiya et al [44] investigated the effect of surface roughness on low cycle fatigue behavior of type 304 stainless steel. In their investigation axial fatigue tests were performed on hourglass shaped specimens in a 593 °C atmosphere. The specimens were heat treated and then artificial surface roughness was applied to the specimens by use of a lathe and silicon carbide paper of different grits. The surface roughness was defined by an RMS value and an R_v value. The results of roughness measurements are summarized in Table 13, where it can be seen that the maximum depth of the surface grooves (R_v) is significantly larger than the RMS value. Figure 36 shows a magnified image of the surface roughness for different degrees of roughness. The authors also suggest that surface roughness has an effect on the early stages of crack growth rate. Figure 37 shows the initial crack growth rate decreases as surface roughness increases. However, the tests data showed that fatigue cracks take less and less time to initiate as surface roughness increases (see Figure 38).

Deng et al [45] evaluated the effect of surface roughness on crack initiation life. They mention that fatigue life is separated into two parts; crack initiation and crack growth. They believe that the effect of surface roughness should be limited to the crack initiation period of fatigue life. In order to validate this, rectangular notched specimens (see Figure 39 for notch geometry) were tested in a three point bending machine at a frequency of 30 Hz with a loading ratio (P_{min}/P_{max}) of $R = 0.05$, and with a true maximum bending stress of 800 MPa at the notch. The notch stress was calculated using finite element analysis. The specimen hardness ranged from 180-230 HB. Three different degrees of surface roughness, 0.03 μm , 0.3 μm and 1.27 μm , were applied to the notch

of the specimens. It should be noted that the roughness parameter used was R_a . Crack initiation was determined by use of ion-sputtered film. When a crack forms in the film, the resistance of the film was increased. Figure 40 shows a plot of the number of cycles versus the average roughness for the total fatigue life, with superimposed curves for crack initiation life and crack growth life. It can be seen in this figure that crack initiation takes up most of the total fatigue life. This figure also shows a decrease in life with an increase in surface roughness; however the differences observed in the crack initiation period are more significant than in the crack growth period. As a result, the authors suggest that the effect of surface roughness should be limited to the crack initiation stage of fatigue life.

7. Summary

Surface finish can have a significant effect on the fatigue behavior of steels. The as-forged surface may have considerable surface roughness, surface decarburization and scale defects. A common surface treatment for as-forged parts is shot cleaning or shot blasting, which is done to clean the surface. This treatment can eliminate some of the detrimental surface effects such as scale and decarburization by removing some of the surface layer and by inducing beneficial compressive residual stresses at the surface. Shot blasting has been found to improve fatigue strength in the HFC region of specimens having rough or as-forged surfaces.

Heat treating is commonly done to forged parts. The process of heat treatment can increase strength (hardness) and lower ductility. There is a near linear relationship between hardness and tensile strength. The endurance strength, or fatigue strength (at 10^7 cycles), increases as the hardness increases for a smooth polished surface. However, there is less change in fatigue strength (at 10^7 cycles) as hardness increases for parts having an as-forged surface condition. In addition, there is an increasing detrimental effect in the LCF region resulting from heat treatment as hardness increases due to reduced ductility.

Decarburization is a gradual reduction of carbon content starting from the surface and can result from heat treatment as well as forging. Decarburization results in a reduction of hardness, or strength, in the decarburized area. There is less of a difference between surface and core hardness as core hardness decreases for heat treated forged specimens. Decarburization can cause a significant reduction in fatigue strength in the HCF region. The reduction in fatigue strength increases as hardness increases. However, as hardness increases beyond 310 HB, surface irregularities may have more of an effect on the fatigue behavior than decarburization. There is less of an effect in the LCF region due to large amounts of plastic deformation. In addition, there is an increasing effect on fatigue behavior with an increase in depth of decarburization. It has been found that decarburization can actually increase fatigue life in the LCF region due to a reduced crack growth rate.

There are many parameters available to define surface roughness. The most commonly used parameter is R_a , the arithmetic average height. However, R_a is not as sensitive to variations in surface roughness as other parameters such as the standard deviation of the distribution of surface heights (R_q), the ten-point height (R_z), or the

maximum height of profile (R_t). It is suggested that R_z and R_t better characterize fatigue behavior as they represent the worst defects in the surface. It is well established that fatigue life in the HCF region decreases as surface roughness increases. It should be noted that surface finish has more of an effect on a harder material.

Fatigue life is often separated into two parts; crack initiation and crack growth. Surface roughness has been shown to have more of an effect on the crack initiation life and it is suggested that the effect of surface roughness should be limited to the crack initiation period. It has been found that the crack initiation life decreases as surface roughness increases. As crack initiation life decreases, the total fatigue life also generally decreases in steels. This is because steels of the same microstructure exhibit the same fatigue crack growth behavior (or crack growth rates).

Several models have been used to evaluate surface finish effect such as the Murakami and the Arola-Ramulu models. The Murakami model treats surface roughness as periodic surface cracks but the Arola-Ramulu model analyzes surface roughness as a notch problem. These models consider surface roughness and do not consider the effects of decarburization. There are also surface finish modification factors which are commonly applied to the endurance strength of the polished condition. However, existing modification factors for the as-forged surface condition, which are based on data dated back to 1930's and 1940's, have been found to be too conservative.

References

- [1] G. H. Farrahi, D. J. Smith, W. X. Zhu, and C. A. McMahon, 2002, "Influence of residual stress on fatigue life of hot forged and shot blasted steel components," *International Journal of Engineering Transactions B: Applications*, Vol. 15, pp. 79-86.
- [2] V. Rudnev, D. Loveless, R. Cook, and M. Black, 2002, *Handbook of Induction Heating*, Marcel Dekker, New York, NY.
- [3] W. Naujoks, 1953, "Forging," *ASME Handbook: Metals Engineering Design*, Vol. 4, pp. 66-74, McGraw-Hill, New York, NY.
- [4] G. Noll and C. Lipson, 1946, "Allowable working stresses," *Proc. Society for Experimental Analysis*, Vol. 3, No. 2, pp. 89-109.
- [5] G. Hankins and M. Becker, 1932, "The fatigue resistance of unmachined forged steels," *Journal of Iron and Steel Institute*, Vol. 126, pp. 205-236.
- [6] G. Hankins, M. Becker, and H. Mills, 1936, "Further experiments on the effect of surface finish conditions on fatigue resistance of steels," *Journal of the Iron and Steel Institute*, Vol. 133, pp. 309-425.

- [7] I. Shareef and M. D. Hasselbusch, 1996, "Endurance limit modifying factors for hardened machined surfaces," *SAE Transactions*, Vol. 105, No. 5, pp. 889-899.
- [8] S. Collins and G. Michal, 1995, "Forging effects on fatigue properties of AISI 4140 steel," *36th MWSP Conf. Proc.*, Vol. 32, pp. 257-269, ISS-AIME, Baltimore, MA.
- [9] Y. Chastel, N. Caillet, and P. Bouchard, 2006, "Qualitative analysis of the impact of forging operations on fatigue properties of steel components," *Journal of Materials Processing Technology*, Vol. 177, pp. 202-205.
- [10] C. Lipson and G. Noll, 1953, "Design practice," *ASME Handbook: Metals Engineering Design*, Vol. 3, pp. 297-305, McGraw-Hill, New York, NY.
- [11] M. Gildersleeve, 1991, "Relationship between decarburization and fatigue strength of through hardened and carburizing steels," *Material Science and Technology*, Vol. 7, pp. 307-310.
- [12] K. Adamaszek and P. Broz, 2001, "Decarburization and hardness changes in carbon steels caused by high temperature surface oxidation in ambient air," *Diffusion and Defect Data: Defect and Diffusion Forum*, Vol. 194, pp. 1701-1706.
- [13] L. C. Leonard and V. Toal, 1998, "Roughness measurements of metallic surfaces based on the laser speckle contrast method," *Optics and Lasers Engineering*, Vol. 30, pp. 433-440.
- [14] E. Abbott, 1940, "The tracer method of measuring surface irregularities," *Surface Treatments*, Vol. 28, pp. 392-427.
- [15] E. S. Gadelmawla, M. M. Koura, T. M. A. Maksoud, I. M. Elewa, and H. H. Soliman, 2002, "Roughness parameters," *Journal of Materials Processing Technology*, Vol. 123, pp. 133-145.
- [16] D. Novovic, R. C. Dewes, D. K. Aspinwall, W. Voice, and P. Bowen, 2004, "Effect of machined topography and integrity on fatigue life," *International Journal of Machine Tools and Manufacture*, Vol. 44, pp. 125-134.
- [17] P. Fluck, 1951, "Influence of surface roughness on the fatigue life and scatter of test results of two steels," *Proceedings of American Society for Testing and Materials*, Vol. 51, pp. 584-592, ASTM, Philadelphia, PA.
- [18] E. Siebel and M. Gaier, 1957, "The influence of surface roughness on the fatigue strength of steels and non-ferrous alloys," *The Engineers' Digest*, Vol. 18, No. 3, pp. 109-112.

- [19] Y. Murakami and M. Endo, 1994, "Effect of defects, inclusions and inhomogenities on fatigue strength," *International Journal of Fatigue*, Vol.16, No. 3, pp. 163-182.
- [20] Y. Murakami, 2002, "Effect of surface roughness on fatigue strength," *Metal Fatigue: Effect of Small Defects and Non Metallic Inclusions*, pp. 28-40, Elsevier, Kidlington, Oxford, UK.
- [21] K. Takahashi and Y. Murakami, 1999, "Quantitative evaluation of effect of surface roughness on fatigue strength," *Engineering Against Fatigue*, pp. 693-703, A.A. Balkema, Ed., Sheffield, UK.
- [22] D. Arola and C. L. Williams, 2002, "Estimating the fatigue stress concentration factor of machined surfaces," *International Journal of Fatigue*, Vol. 24, pp. 923-930.
- [23] R. I. Stephens, A. Fatemi, R. R. Stephens, and H. O. Fuchs, 2000, *Metal Fatigue in Engineering*, 2nd Ed., John Wiley and Sons, New York, NY.
- [24] R. Budynas and J. Nisbett, 2008, *Shigley's Mechanical Engineering Design*, 8th Ed., McGraw Hill, New York, NY.
- [25] C. Lipson and R. Juvinall, 1963, *Handbook of Stress and Strength*, pp. 99-113, Macmillan, New York, NY.
- [26] K. Edwards and R. McKee, 1991, *Fundamentals of Mechanical Component Design*, McGraw-Hill, New York, NY.
- [27] R. Norton, 2000, *Machine Design*, Prentice Hall, Upper Saddle River, NJ.
- [28] R. Juvinall and K. Marshek, 1991, *Fundamentals of Machine Component Design*, 2nd Ed., John Wiley and Sons, Hoboken, NJ.
- [29] A. Burr and J. Cheatham, 1995, *Mechanical Analysis and Design*, 2nd Ed., Prentice Hall, Englewood Cliffs, NJ.
- [30] N. Dowling, 1998, *Mechanical Behavior of Materials: Engineering Methods for Deformation, Fracture, and Fatigue*, 2nd Ed., Prentice Hall, Upper Saddle River, NJ.
- [31] J. Bannantine, J. Comer, and J. Handrock, 1990, *Fundamentals of Metal Fatigue Analysis*, Prentice Hall, Englewood Cliffs, NJ.
- [32] R. Heywood, 1962, *Designing Against Fatigue*, Chapman and Hall, London, England.

- [33] B. C. Hanley and T. J. Dolan, 1953, "Surface finish," *ASME Handbook: Metals Engineering Design*, Vol. 3, pp. 100-106, McGraw-Hill, New York, NY.
- [34] H. Wiegand, 1940, "Effect of surface treatment on fatigue strength," *MAP Translation 1772*, BMW, Flugmtorenbau, Berlin.
- [35] R. Z. Manteuffel, 1941, "Fatigue endurance of power vehicle springs and possibilities of influencing same," *Deut. Kraftfahrforsch*, Vol. 49, pp. 1-51.
- [36] F. Zimmerli, 1944, "Shot blasting and its effect on fatigue life," *Surface Treatments of Metals*, American Society for Metals, pp. 261-278.
- [37] Nicholson, 1967, *Heat Treatment of Steels*, Vol. 61, Dept. of Scientific and Industrial Research, Wellington, New Zealand.
- [38] G. E. Totten, 2007, *Steel Heat Treatment Handbook*, CRC Press, Boca Raton, FL.
- [39] G. E. Totten and M. Howes, 1997, *Steel Heat Treatment Handbook*, pp. 251-292, Marcell Dekker, New York, NY.
- [40] D. Callister, 2003, *Material Science and Engineering an Introduction*, 6th Ed., John Wiley and Sons, Hoboken, NJ.
- [41] R. Landgraf, 1968, "Cyclic deformation and fatigue behavior of hardened steels," *TAM Report*, No. 320, pp. 1-98, University of Illinois, Department of Theoretical and Applied Mechanics, Urbana, Illinois.
- [42] J. M. Barsom, 1971, "Fatigue-crack propagation in steels of various yield strengths," *Trans. ASME, J. Eng. Ind.*, Ser. B, No. 4, pp. 1190-1196.
- [43] A. Ariel and A. Mukherjee, 1979, "Decarburization and fatigue," *The Enigma of the Eighties: Environment, Economics, Energy*, Vol. 1, pp. 103-111.
- [44] P. Maiya and D. Busch, 1975, "Effect of surface roughness on low cycle fatigue behavior of type 304 stainless steel," *Metallurgical Transactions A*, Vol. 6A, pp. 1761-1766.
- [45] G. Deng, K. Nagamoto, Y. Nakano, and T. Nakanishi, 2009, "Evaluation of the effect of surface roughness on crack initiation life," *ICF12*, pp. 1-8, Natural Resources Canada, Ottawa, Canada.

Table 1: Hardness variation between surface and subsurface for four types of forged steels used in fatigue tests in [5].

Description of Material	Manufacturer	Diamond Pyramid Hardness		
		At Surface	Interior	Difference
0.20% carbon steel	A	150	154	4
	B	146	158	12
0.40% carbon steel	A	206	221	15
	B	171	192	21
3% nickel steel	A	233	284	51
	B	215	247	32
nickel-chromium steel	A	201	333	42
	B	242	289	47

Table 2: Fatigue test results for four types of commonly used forged steels with the as-forged and machined and polished surface conditions used in [5].

Material	Manufacturer	Average Brinell Hardness Number (1)	Tensile Strength, Tons per sq. in. (2)	Endurance Fatigue Limit, Tons per sq. in.		Ratio Col. (3) Col. (4)	Ratio Col. (3) Col. (2)	Ratio Col. (4) Col. (2)
				As-Forged (3)	Machined and Polished (4)			
0.20% carbon steel	A	135	30	± 12.1	± 14.2	0.85	0.40	0.47
	B	149	33	± 11.7	± 14.7	0.80	0.35	0.45
0.40% carbon steel	A	205	45	± 16.5	± 21.0	0.78	0.37	0.47
	B	185	41	± 12.7	± 21.6	0.59	0.31	0.53
3% nickel steel	A	274	59	± 15.0	± 32.5	0.46	0.25	0.55
	B	240	52	± 15.8	± 27.9	0.57	0.31	0.54
nickel-chromium	A	308	66	± 18.0	± 31.5	0.57	0.27	0.48
	B	278	60	± 14.4	± 31.0	0.46	0.24	0.52

Table 3: Fatigue test results for a high strength forged steel from two manufacturers with the as-forged and machined and polished surface conditions used in [6].

Manufacturer	Tensile Strength, Tons per sq. in. (1)	Endurance Fatigue Limit, Tons per sq. in.		Ratio Col. (2) Col. (3)	Ratio Col. (2) Col. (1)	Ratio Col. (3) Col. (1)
		As-Forged (2)	Machined and Polished (3)			
B	118	± 9.4	± 49.5	0.19	0.08	0.42
C	138	± 8.3	± 49.5	0.17	0.06	0.36

Table 4: Relationship between surface carbon content, depth of decarburization, and fatigue limit for a 605 M36 through-hardened steel [11].

Surface carbon content, wt-%	Depth of decarburisation, mm	Fatigue limit, MN m ⁻²
0.1	0.7	450
	1.0	400
0.15	0.4	480
	1.0	480
0.2	0.4	530
	0.7	530

Table 5: Summary of endurance limits and tensile strengths for ground, machined, hot-rolled, and as-forged surface conditions used to calculate surface finish factors from [4].

Figure No.	Brinell Hardness	Tensile Strength psi	Yield Point psi	ENDURANCE LIMIT—PSI			
				Ground Surface	Machined Surface	Hot Rolled Surface	As-Forged Surface
11	160–187	77,000	48,000	33,000	30,000	24,000	18,000
12	187–207	89,000	60,000	39,000	34,000	25,000	19,000
13	207–217	99,000	69,000	44,000	37,000	27,000	20,000
14	217–229	103,000	74,000	46,000	38,000	27,000	20,000
15	229–241	109,000	80,000	49,000	40,000	28,000	20,000
16	241–255	114,000	86,000	51,000	42,000	29,000	21,000
17	255–269	121,000	94,000	55,000	44,000	30,000	21,000
18	269–285	127,000	101,000	57,000	46,000	30,000	22,000
19	285–302	135,000	110,000	61,000	49,000	31,000	22,000
20	302–321	142,000	120,000	64,000	51,000	32,000	23,000
21	321–352	151,000	130,000	68,000	53,000	33,000	23,000
22	352–375	166,000	147,000	74,000	57,000	34,000	24,000
23	375–401	176,000	158,000	78,000	59,000	35,000	25,000
24	401–429	188,000	171,000	82,000	62,000	35,000	24,000
25	429–461	202,000	183,000	86,000	64,000	35,000	24,000
26	461–495	217,000	196,000	88,000	65,000	34,000	22,000
27	495–514	233,000	210,000	89,000	66,000	32,000	20,000
28	514–555	241,000	217,000	89,000	65,000	31,000	19,000

Table 6: Values of $\sqrt{area_R}$ parameter used in Murakami equation to predict fatigue limit for specimens which have surface roughness defects [20].

Specimen	$R_p/2b$	$\sqrt{area_R}/2b$	$\sqrt{area_R} \mu\text{m}$
100A	0.273	0.38	38
150A	0.443	0.38	57
200A	0.370	0.38	76
150QT	0.137	0.32	47

Table 7: Results of experimental and predicted fatigue limits using the Murakami equation for JIS S45C steel specimens having surface roughness defects [20].

(a) Annealed specimens						
Specimen	HV	$\sqrt{area_R} \mu\text{m}$	● broken ○ not broken	depth of crack initiation site μm	Experiment σ_a MPa	Prediction σ_w MPa
E P	170 ± 10	—	●	0	284	$272 \pm 16^*$
			●	0	265	
			○	—	260	
			○	—	255	
			○	—	245	
100A	180 ± 10	38	●	17	255	234 ± 8
			●	14	250	
			○	—	245	
			○	—	235	
			○	—	216	
150A	180 ± 10	57	●	32	245	219 ± 7
			○	—	235	
			○	—	216	
200A	180 ± 10	76	●	78	235	208 ± 7
			○	—	230	
			○	—	226	
Single notch	170 ± 10	95**	●	32	196	194 ± 7
			●	31	186	
			○	—	181	
			○	—	177	

* Predicted using equation (16.5). ** Predicted using equation (2.9) for $a = 30 \mu\text{m}$

(b) Quenched and tempered specimens						
Specimen	HV	$\sqrt{area_R} \mu\text{m}$	● broken ○ not broken	depth of crack initiation site μm	Experiment σ_a MPa	Prediction σ_w MPa
150QT	650 ± 30	47	●	17	608	580 ± 22
			●	18	569	
			○	—	549	
			○	—	530	

Table 8: Surface finish modification factors at 10^4 and 10^6 cycles for hardened machined surfaces calculated using the Goodman, Morrow, and SWT models [7].

LIFE CYCLES	METHOD USED		
	Goodman	Morrow	SWT
10,000	0.75	1	0.97
1,000,000	0.75	0.82	0.85

Table 9: Constants for use in Eqn. 22 for determining surface finish factors for ground, machined, hot-rolled, and as-forged surfaces [24].

Surface Finish	Factor a		Exponent b
	S_{ut} , kpsi	S_{ut} , MPa	
Ground	1.34	1.58	-0.085
Machined or cold-drawn	2.70	4.51	-0.265
Hot-rolled	14.4	57.7	-0.718
As-forged	39.9	272.	-0.995

From C.J. Noll and C. Lipson, "Allowable Working Stresses," *Society for Experimental Stress Analysis*, vol. 3, no. 2, 1946 p. 29. Reproduced by O.J. Horger (ed.) *Metals Engineering Design ASME Handbook*, McGraw-Hill, New York. Copyright © 1953 by The McGraw-Hill Companies, Inc. Reprinted by permission.

Table 10: Fatigue test results on as-forged, as-forged/shot blasted, forged/heat treated, and forged/ heat treated/ shot blasted specimens of EN15R steel [1].

Batch	Weibull Slope β	Characteristic Life (cycles)
$\Delta\epsilon/2 = 2200 \mu\epsilon$		
AF	4.82	89,809
FS	5.36	140,271
HT	11.27	91,378
HTS	2.04	500,453
$\Delta\epsilon/2 = 6000 \mu\epsilon$		
AF	5.97	3,820
FS	4.69	3,470
HT	11.44	2,724

AF = as-forged, without heat treatment and shot blasting

HT = forged, heat treated without shot blasting

FS = forged and shot blasted without heat treatment

HTS = forged, heat treated, and shot blasted

Table 11: List of typical heat treatment procedures for steels [37].

Treatment	Details	Objective
1. Annealing (a.) Full annealing	Austenitise, ($A_3+30-50^\circ\text{C}$) and furnace cool.	Soften hypo-eutectoid steel for machining or cold working.
(b.) Spheroidising anneal	Heat below A_3 .	Spheroidise carbides making steels amenable to cold forming processes, and higher carbon steels suitable for machining.
(c.) Stress relief anneal	Heat in range $550-650^\circ\text{C}$.	Relieve internal stresses due to machining, welding or cold working.
2. Normalising	Austenitise, ($A_3+30-50^\circ\text{C}$) and cool in air.	Refine grain size and improve uniformity of structure.
3. Quenching and Tempering	Austenitise, ($A_3+30-50^\circ\text{C}$), rapidly cool. Reheat at intermediate temperature, e.g. $300-400^\circ\text{C}$.	Obtain best combination of strength and ductility. By varying the tempering temperature possible to obtain desired properties within a wide range.
4. Austempering	Quench from austenite region to a temperature suitable for bainite formation.	Obtain greater ductility while maintaining high hardness. Process restricted to small components.
5. Martempering	Quench from austenite region to a temperature just above M_s , air cool to room temperature. Temper at intermediate temperature.	Process gives similar properties to quenching and tempering, but greatly reduces possibility of distortion and quench cracks.

Table 12: Material conditions, test parameters and fatigue lives for notched 4340 low alloy steel specimens with and without decarburization [43].

Test No.	a_o (in)	a_d (in)	a_n (in)	$\sigma_{surface}$ (ksi)	σ_{max} (ksi)	$\Delta\sigma$ (ksi)	N_d	N_b	N_t	Remarks
1	1.0	0	2.5	140	50	10	0	∞	∞	$\Delta K < \Delta K_{th}$
2	1.0	0	2.5	140	50	30	0	23,786	23,786	
3	1.0	0	2.5	140	50	50	0	7,540	7,540	
4	1.0	0	1.1	140	75	10	0	∞	∞	$\Delta K < \Delta K_{th}$
5	1.0	0	1.1	140	75	30	0	1,880	1,880	
6	1.0	0	1.1	140	75	50	0	595	595	
7	1.001	1.01	2.5	20	50	10	38,783	281,680	320,463	
8	1.001	1.01	2.5	20	50	30	3,274	23,781	27,055	
9	1.001	1.01	2.5	20	50	50	1,037	7,535	8,572	
10	1.002	1.01	1.1	20	75	10	34,474	21,155	55,629	
11	1.002	1.01	1.1	20	75	30	2,911	1,786	4,697	
12	1.002	1.01	1.1	20	75	50	922	566	1,488	
13	1.002	1.1	2.5	20	50	10	422,310	233,370	655,680	
14	1.002	1.1	2.5	20	50	30	34,438	19,703	54,141	
15	1.002	1.1	2.5	20	50	50	10,911	6,243	17,514	
16	1.004	1.1	1.1	20	75	10	413,690	0	413,690	
17	1.004	1.1	1.1	20	75	30	32,990	0	32,990	
18	1.004	1.1	1.1	20	75	50	10,453	0	10,453	
19	1.003	1.5	2.5	20	50	10	677,470	113,920	791,390	
20	1.003	1.5	2.5	20	50	30	57,196	9,618	66,814	
21	1.003	1.5	2.5	20	50	50	18,122	3,047	21,159	
22	1.006	1.5	1.5	20	75	10	650,800	0	650,800	
23	1.006	1.5	1.5	20	75	30	52,757	0	52,757	
24	1.006	1.5	1.5	20	75	50	17,314	0	17,314	

Table 13: Roughness measurements for various types of surface preparations in type 304 stainless steel [44].

Surface Preparation	Surface Roughness R, μm (rms)	Maximum Depth of Surface Grooves, μm
Ground on silicon carbide paper		
600 grit	0.045	0.18
240 grit	0.48	1.8
50 grit	2.9	8.9
Polished		
Mechanically	~ 0.0075	< 0.027
Electrolytically	~ 0.0075	< 0.027

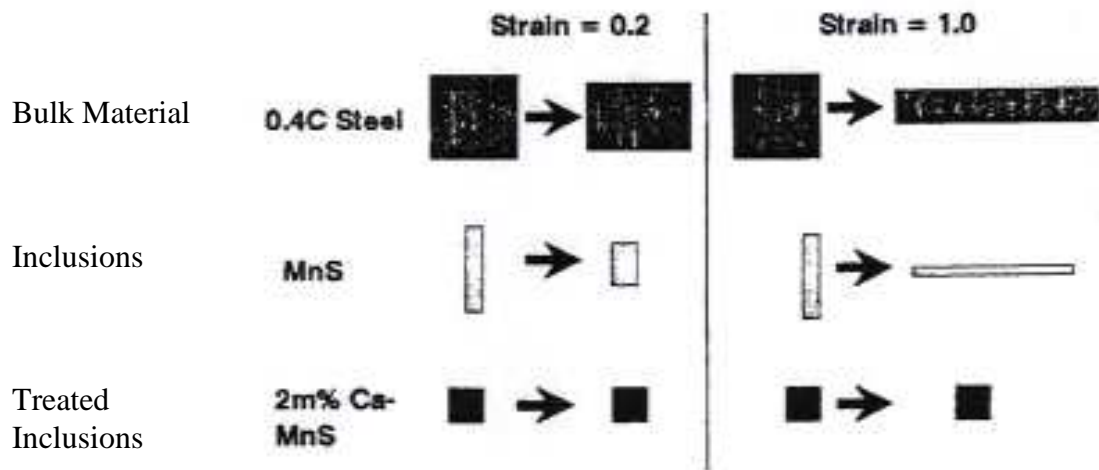


Figure 1: The relative shape change of treated and untreated inclusions compared to shape change of the steel billet for strains of 0.2 and 1.0 at 1000°C [8].

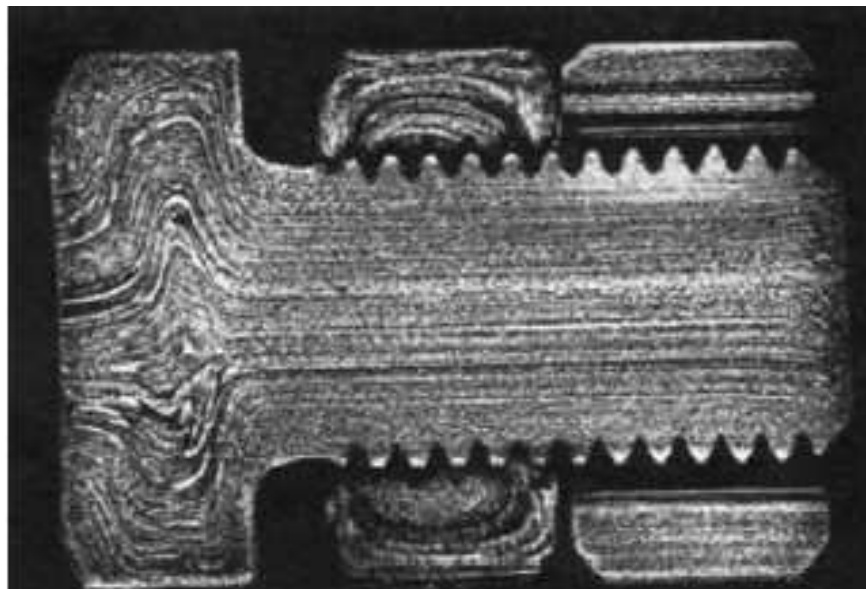


Figure 2: Illustration of a cross section of a forged steel part showing grain flow [9].

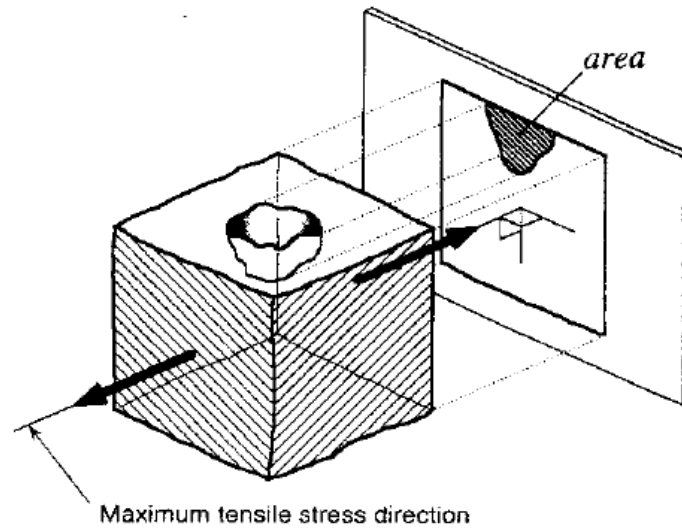


Figure 3: Projection of a defect onto a plane perpendicular to maximum tensile stress which is used to calculate the square root area parameter [19].

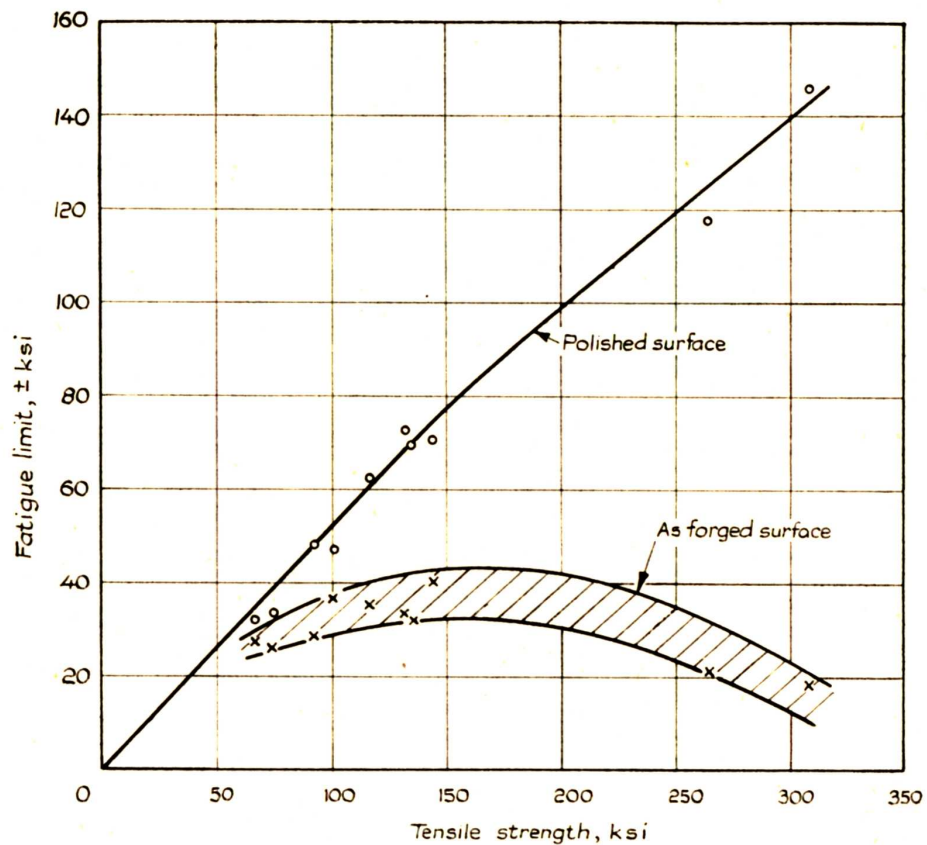
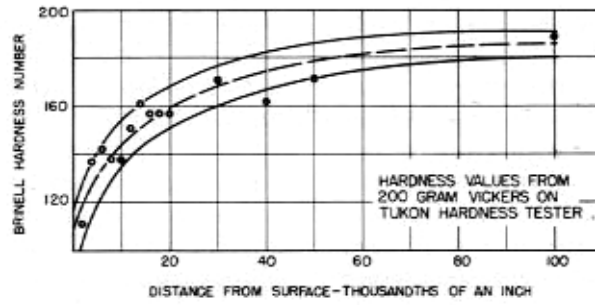
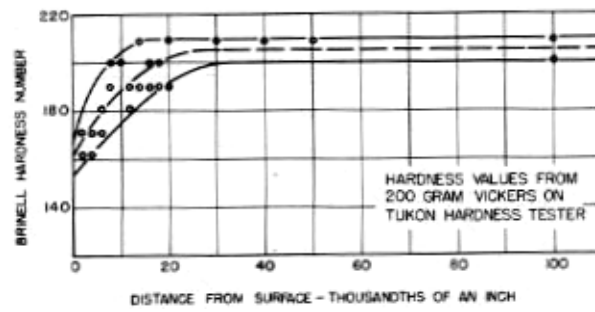


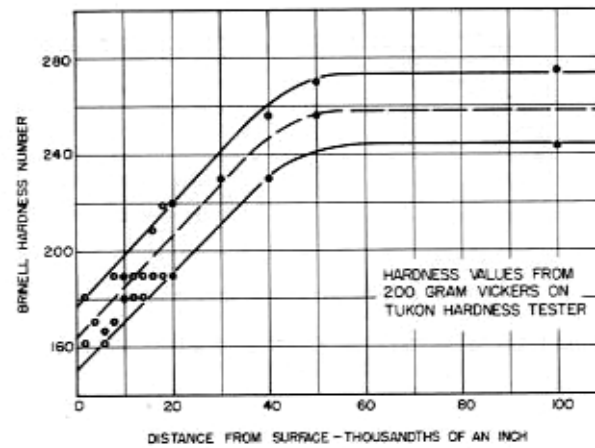
Figure 4: Endurance limit versus tensile strength for as-forged surface finish and polished surface finish specimens [32].



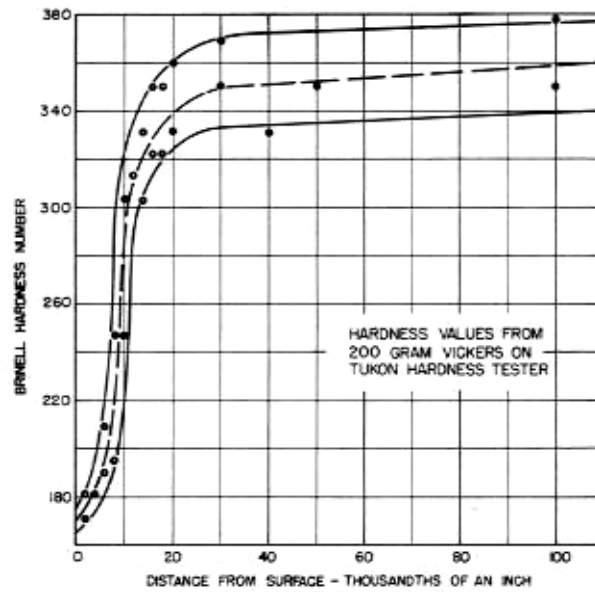
(a)



(b)

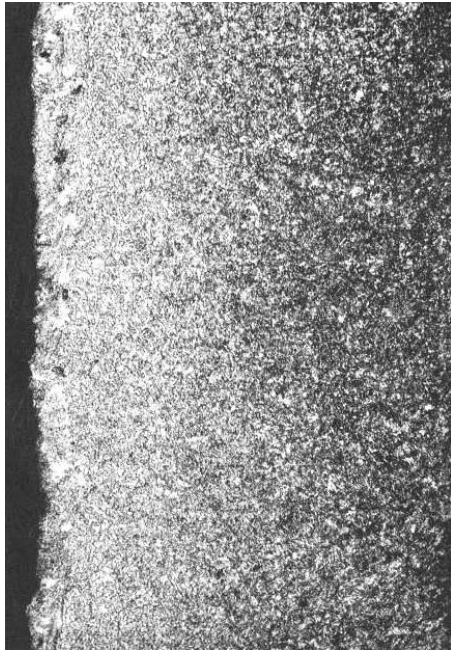


(c)

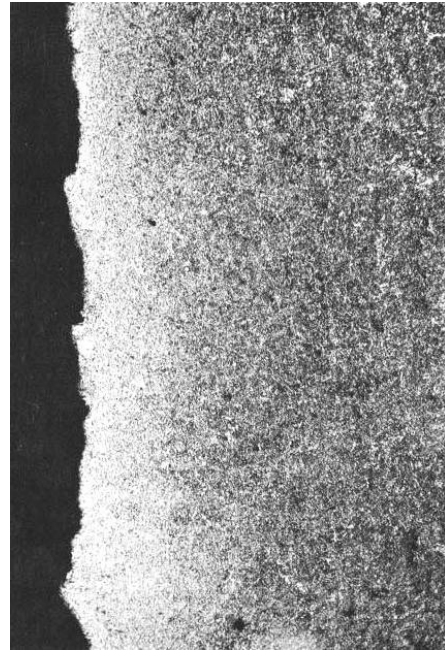


(d)

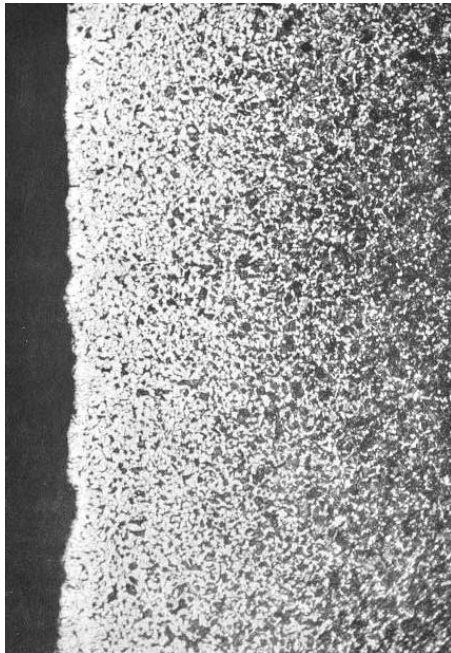
Figure 5: Brinell hardness versus distance from surface for as-forged specimens with average core hardness of (a) 185 HB, (b) 200 HB, (c) 260 HB, and (d) 360 HB [4].



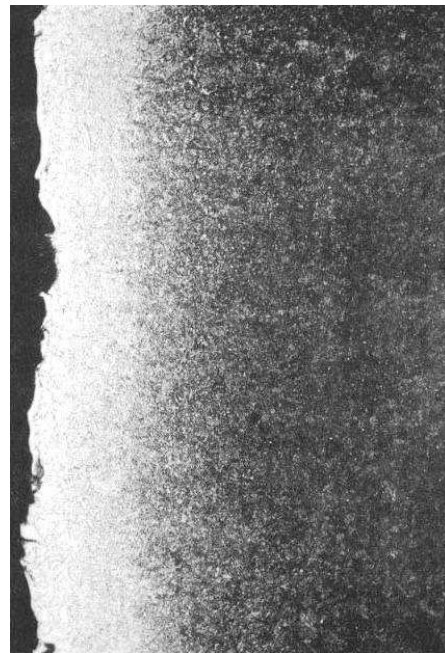
(a)



(b)



(c)



(d)

Figure 6: Magnified images (150 x magnification) of a cross section of as-forged specimens showing surface decarburization with average core hardness of (a) 185 HB and decarburization ranging from 0.64 mm to 0.76 mm, (b) 200 HB and decarburization ranging from 0.25 mm to 0.30 mm, (c) 260 HB and decarburization ranging from 0.76 mm to 0.89 mm, and (d) 360 HB and decarburization ranging from 0.30 mm to 0.38 mm [4].

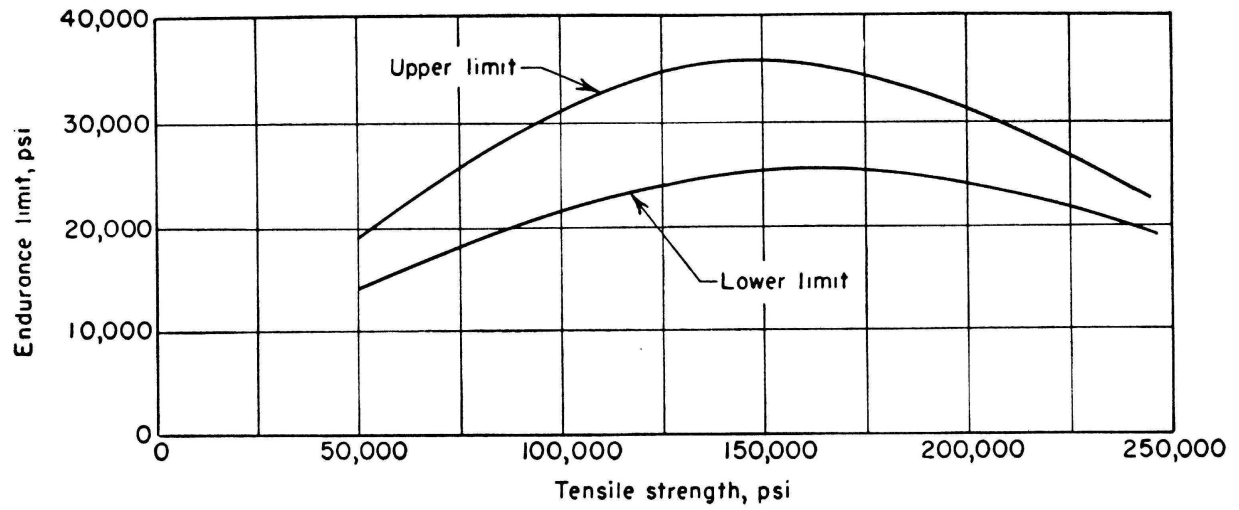


Figure 7: Endurance limit versus tensile strength showing upper and lower limits for as-forged surface specimens [10].

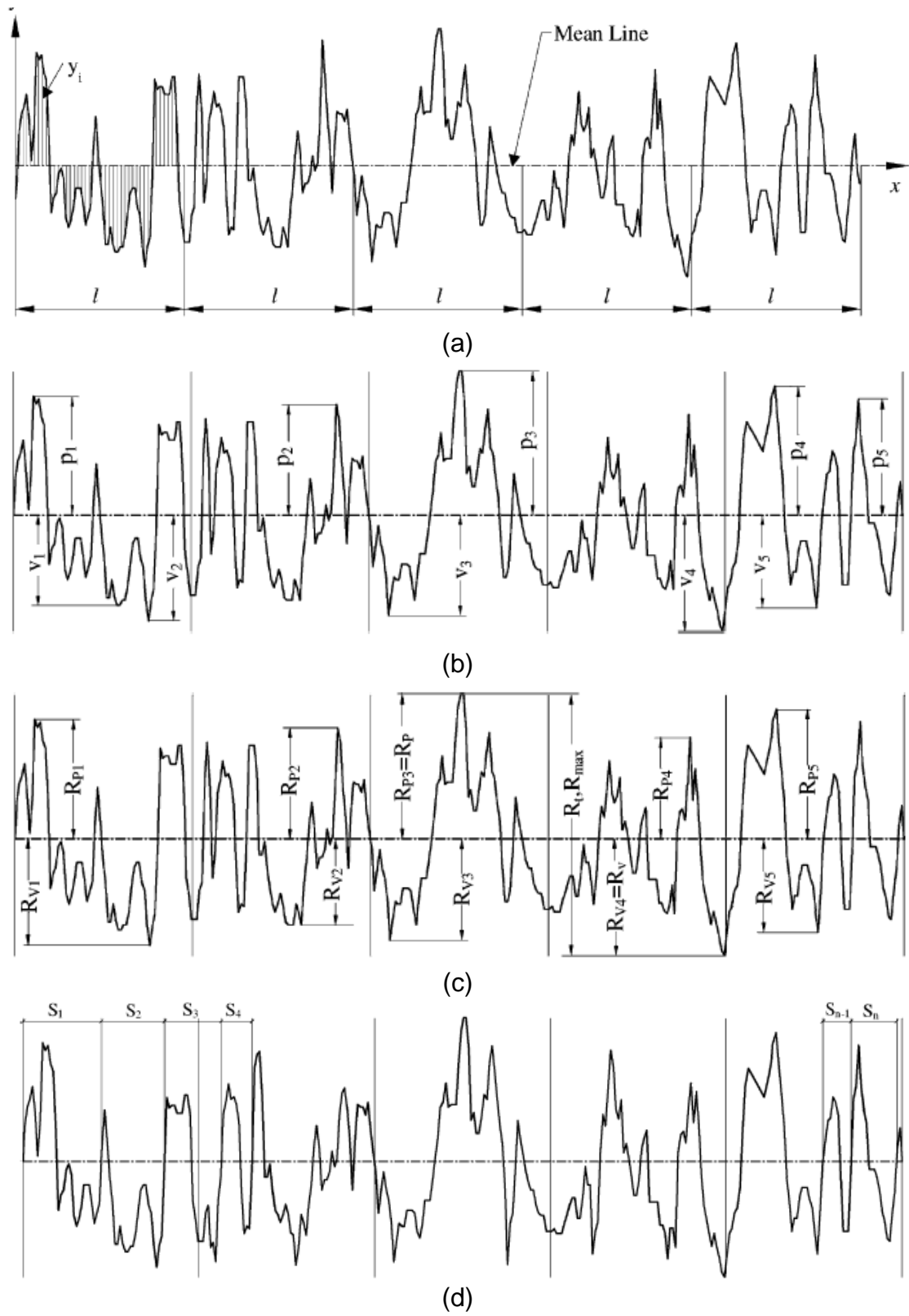


Figure 8: Definition of (a) R_a , (b) R_z , (c) R_t and R_y , and (d) S_m to characterize surface roughness [15].

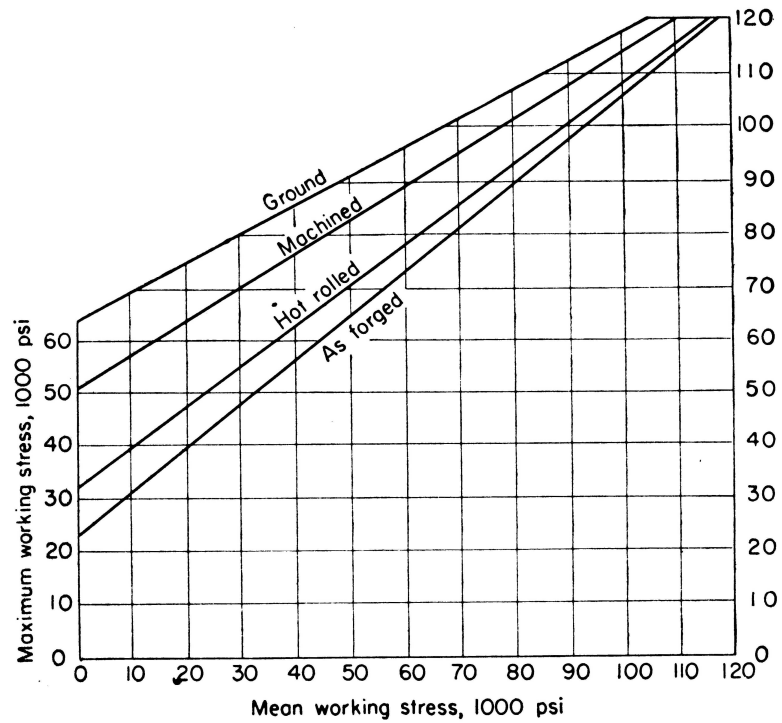


Figure 9: Maximum working stress (at 10^7 cycles) versus mean working stress (at 10^7 cycles) for the ground, machined, hot-rolled and as-forged surface conditions of steel (302 HB-321 HB) [4].

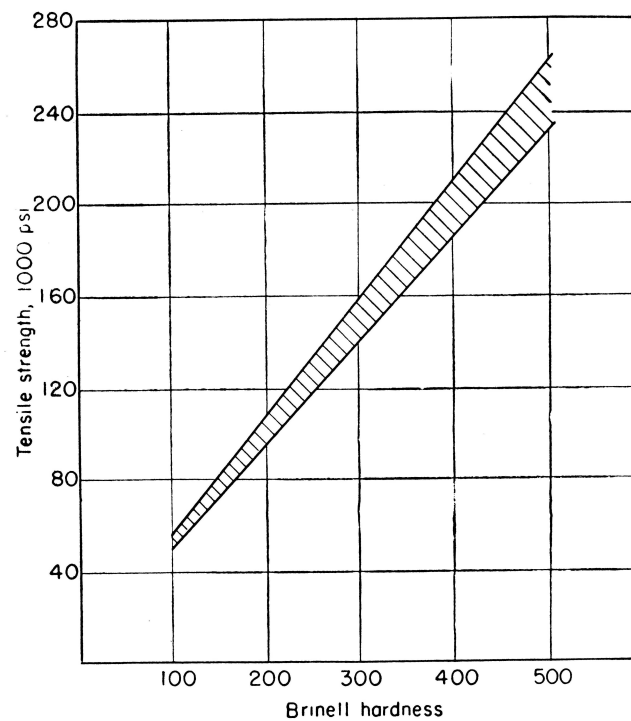


Figure 10: Relationship between Brinell hardness and tensile strength for steels [4].

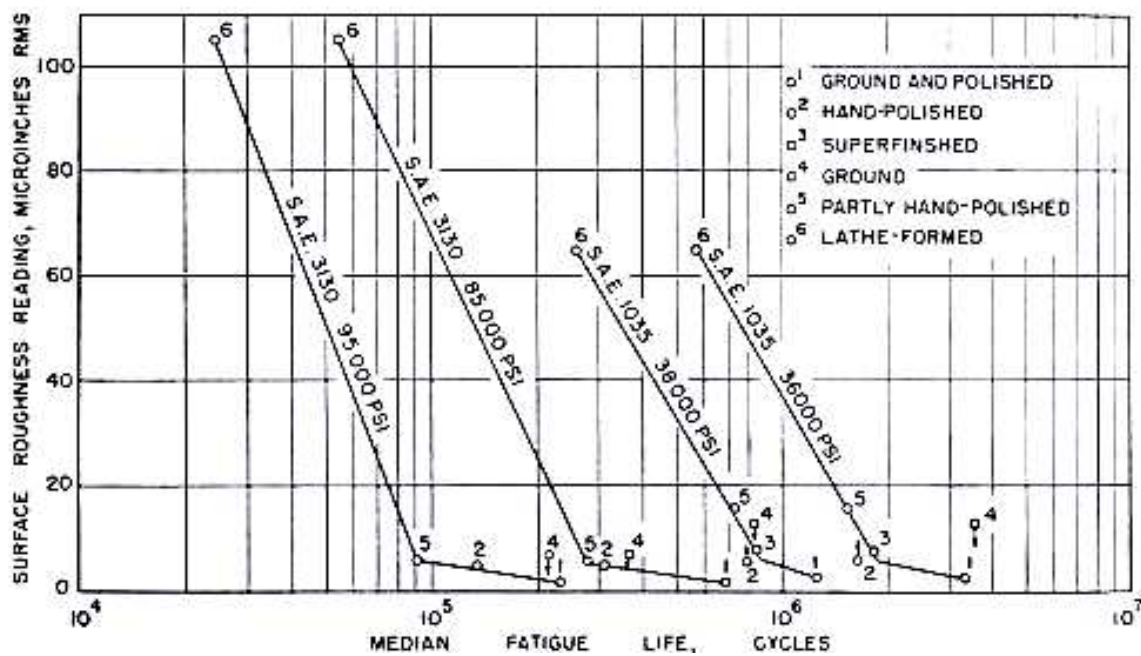
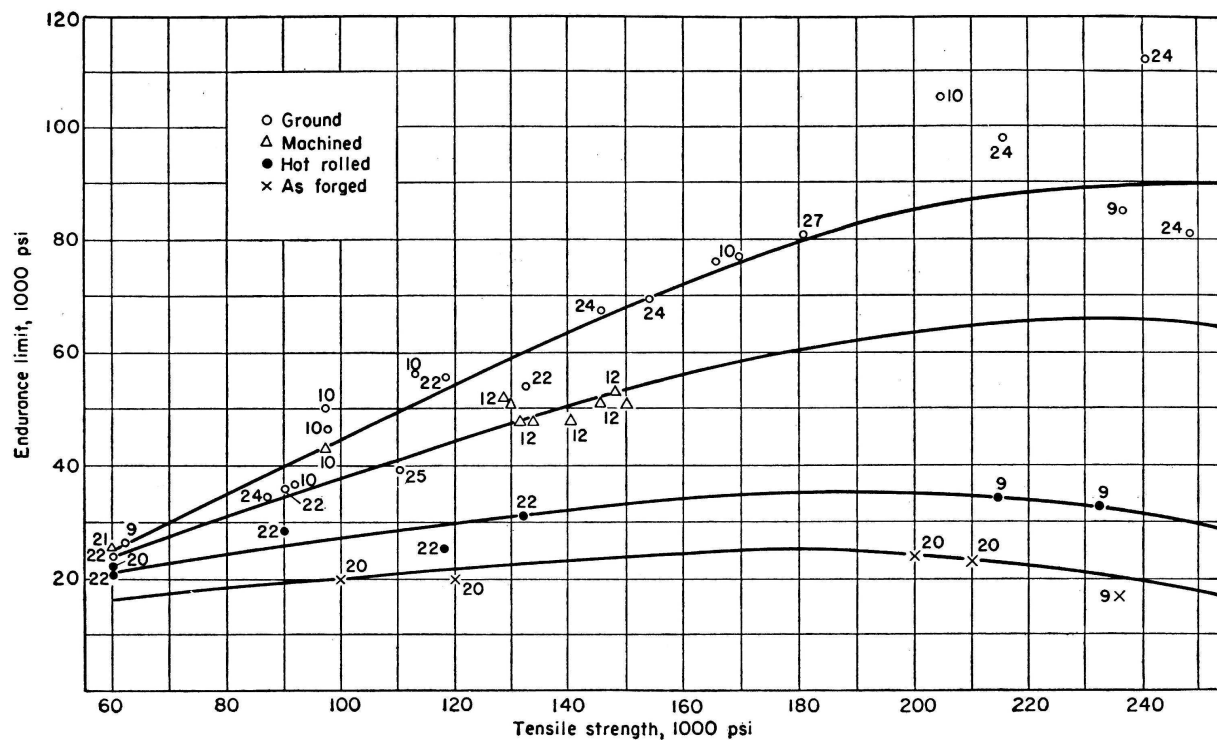


Figure 12: Surface roughness versus median fatigue life for SAE 1035 and SAE 3130 steels [17].

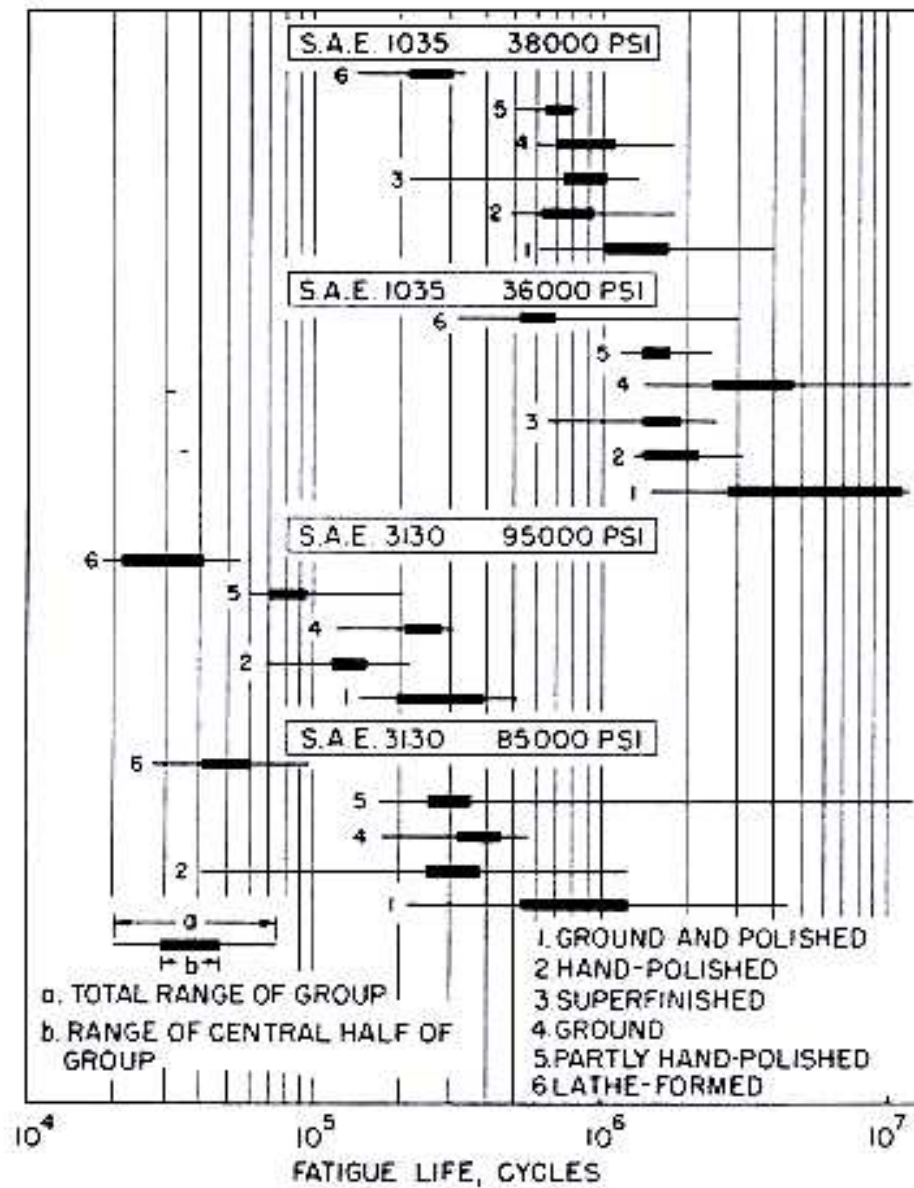


Figure 13: Scatter of fatigue test results for SAE 1035 and SAE 3130 steels having a range of surface roughness [17].

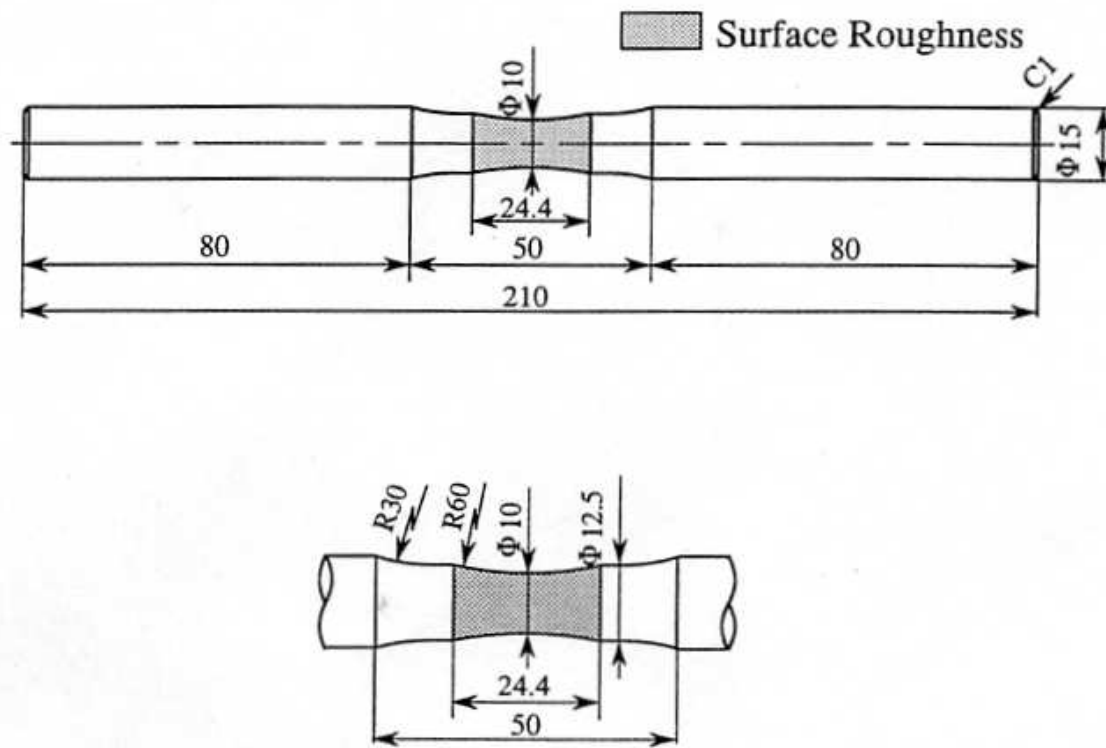


Figure 14: Configuration and dimensions (mm) of JIS S45C steel fatigue specimens used in [20].

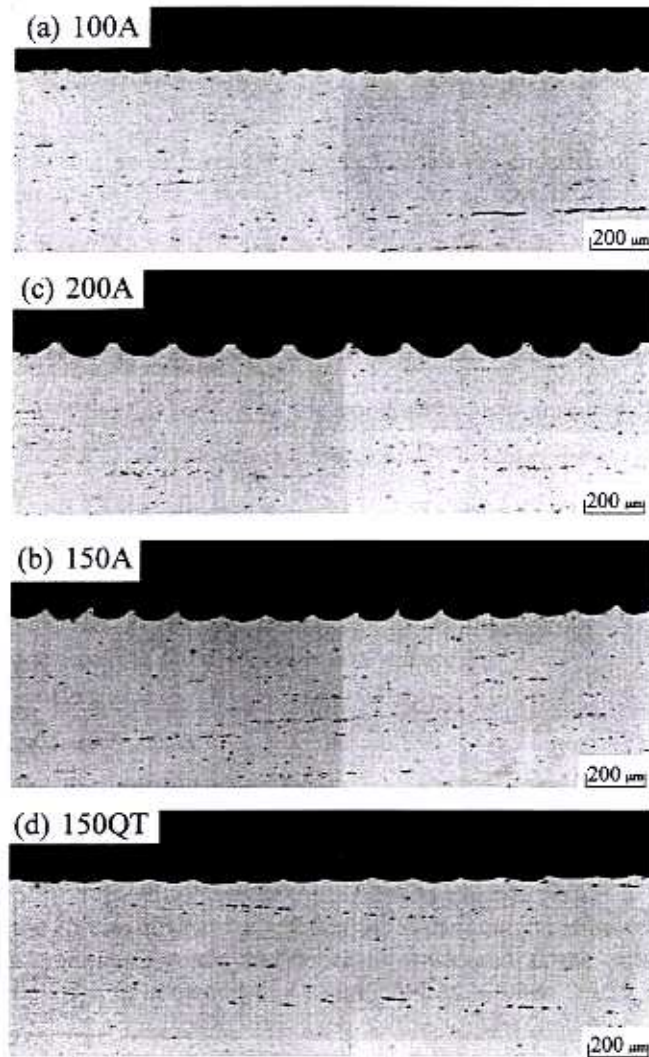


Figure 15: Magnified image of artificially induced surface roughness for annealed (A) and quenched and tempered (QT) JIS S45C steel with roughness pitch at 100, 150 and 200 in [20].

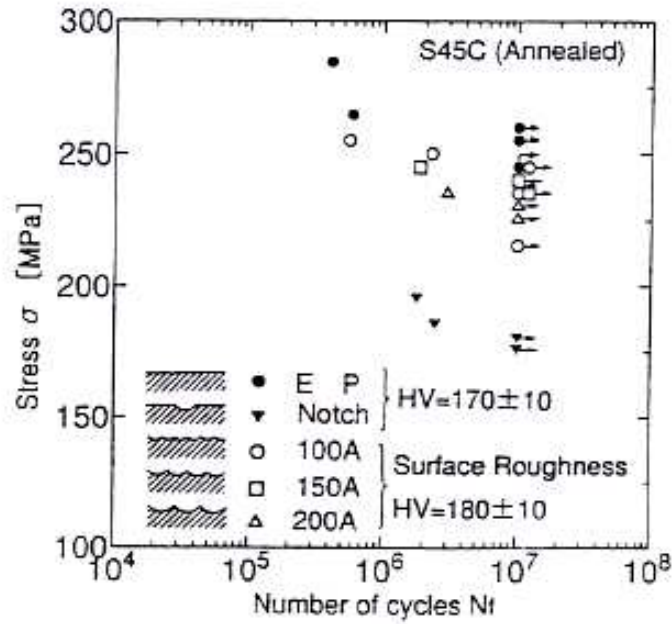


Figure 16: Composite plot of stress versus fatigue life for different types of roughness in JIS S45C steel specimens [20].

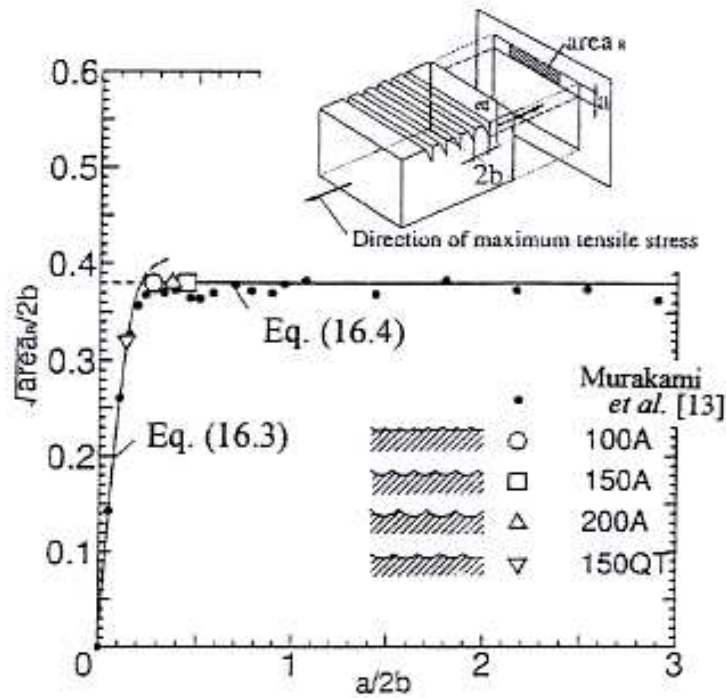


Figure 17: Relationship between $\sqrt{\text{area}_r}/2b$ and $a/2b$ for annealed (A) and quenched and tempered (QT) JIS S45C steel fatigue specimens [20].

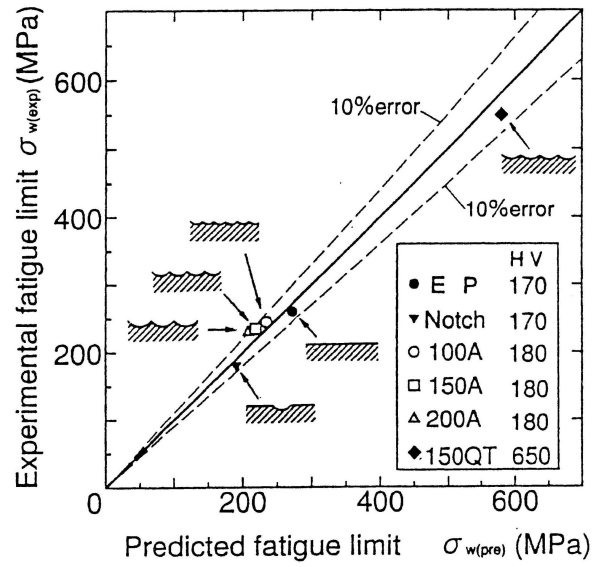


Figure 18: Relationship between predicted and experimental fatigue limits for annealed and quenched and tempered JIS S45C steel [20].

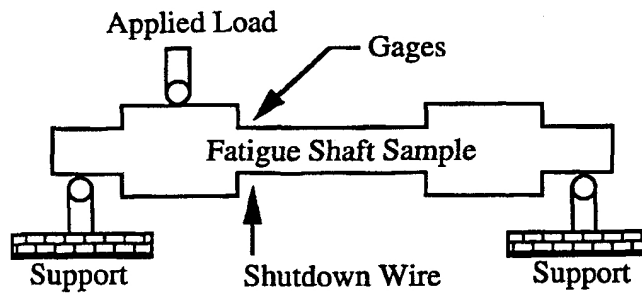


Figure 19: Specimen geometry and test set up for the hardened SAE 4140 steel shaft subjected to bending fatigue in [7].

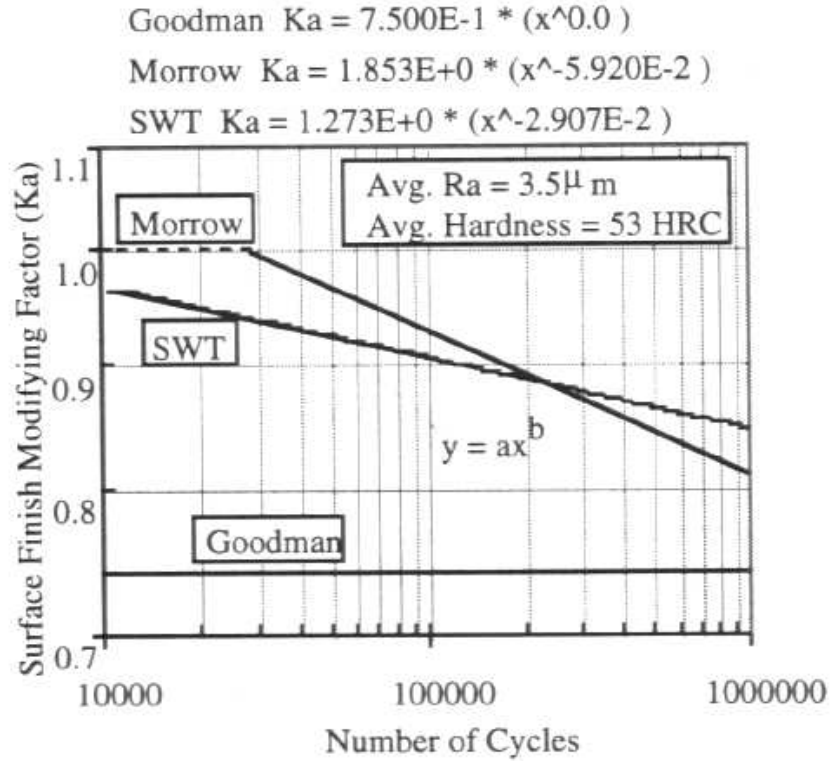


Figure 20: Surface finish modification factors for fatigue life ranging from 10^4 to 10^6 cycles for hardened machined surfaces calculated using the Goodman, Morrow, and SWT models for hardened machined steel surfaces [7].

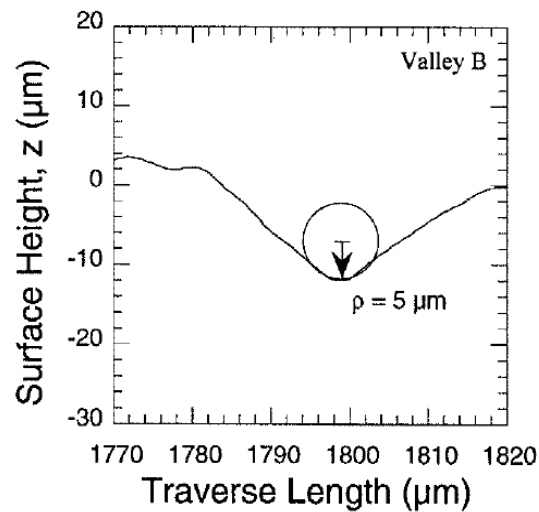


Figure 21: Roughness profile showing definition of the parameter $\bar{\rho}$ (average radius of the dominant profile valleys) used in Arola-Ramulu Model [22].

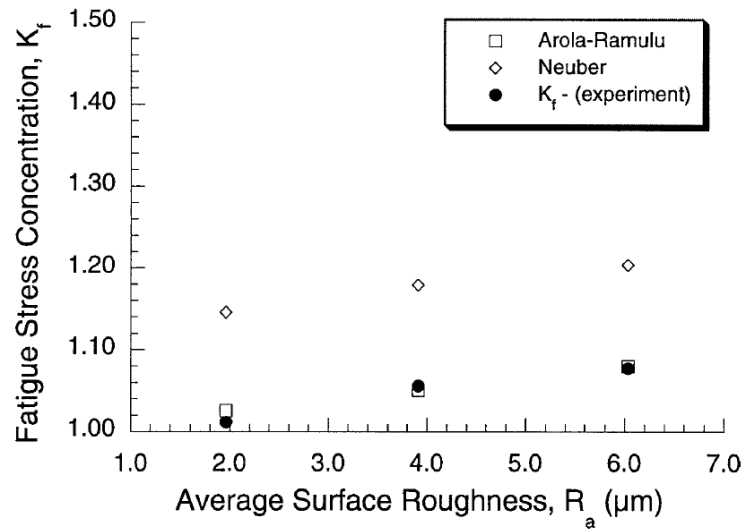


Figure 22: Fatigue stress concentration factor calculated using Arola-Ramulu and Neuber models, and experimental fatigue stress concentration factor versus average surface roughness for a high strength low alloy steel [22].

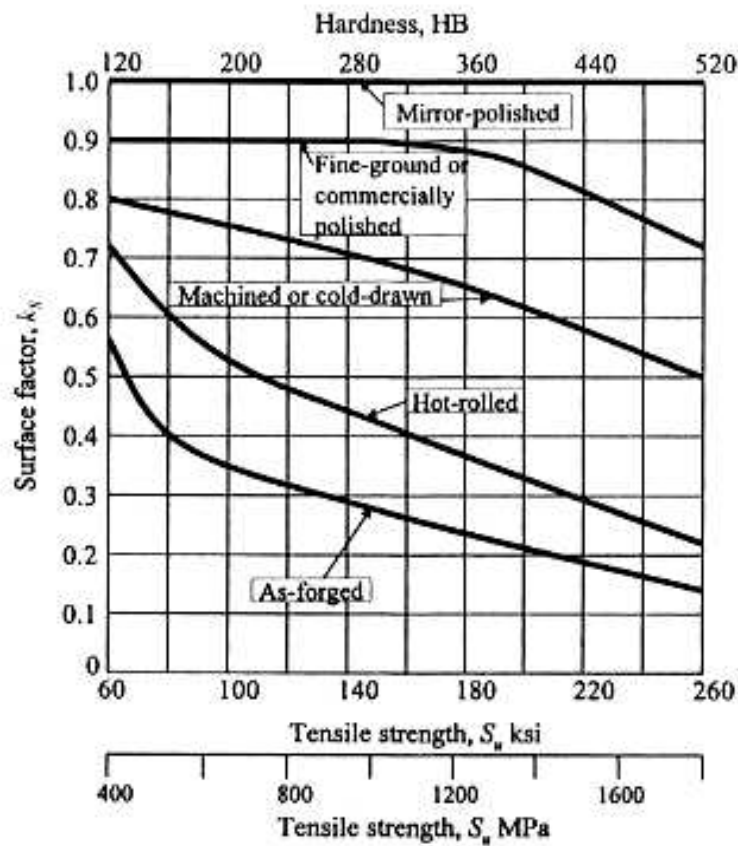


Figure 23: Surface finish modification factor versus tensile strength or Brinell hardness for ground and polished, machined, hot-rolled, and as-forged surface conditions [23].

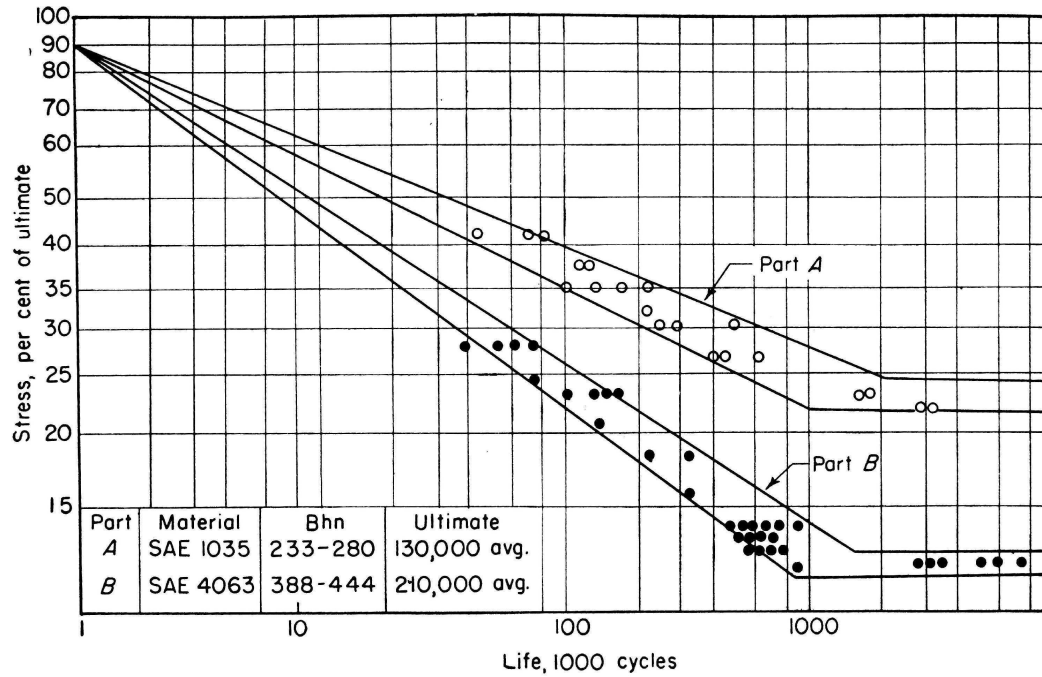


Figure 24: Stress versus cycles to failure for two type of as-forged surface finish specimens made from SAE 1035 steel (233 HB-280 HB) and SAE 4063 steel (388 HB-444 HB) [10].

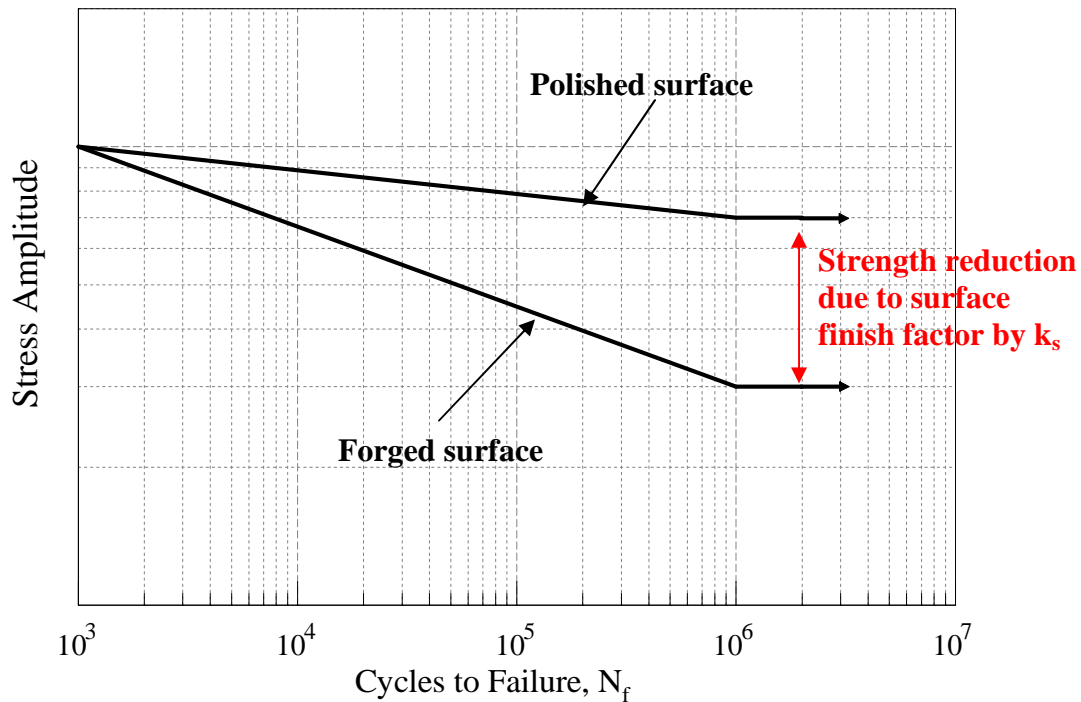


Figure 25: Stress amplitude versus cycles to failure for steel specimens having machined and polished surface and as-forged surface conditions.

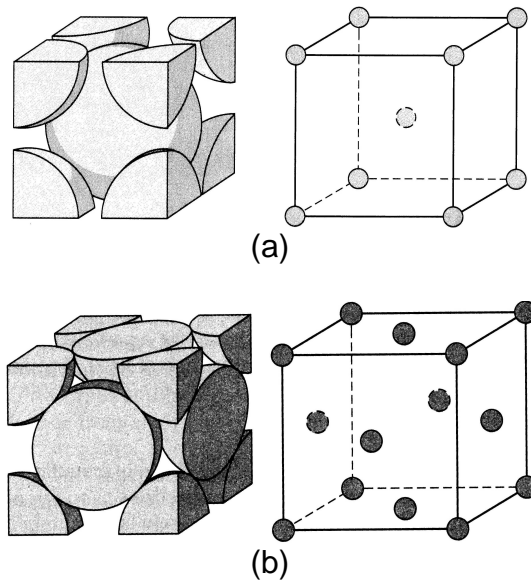


Figure 26: Atomic structure of iron showing (a) body centered cubic, and (b) face centered cubic [40].

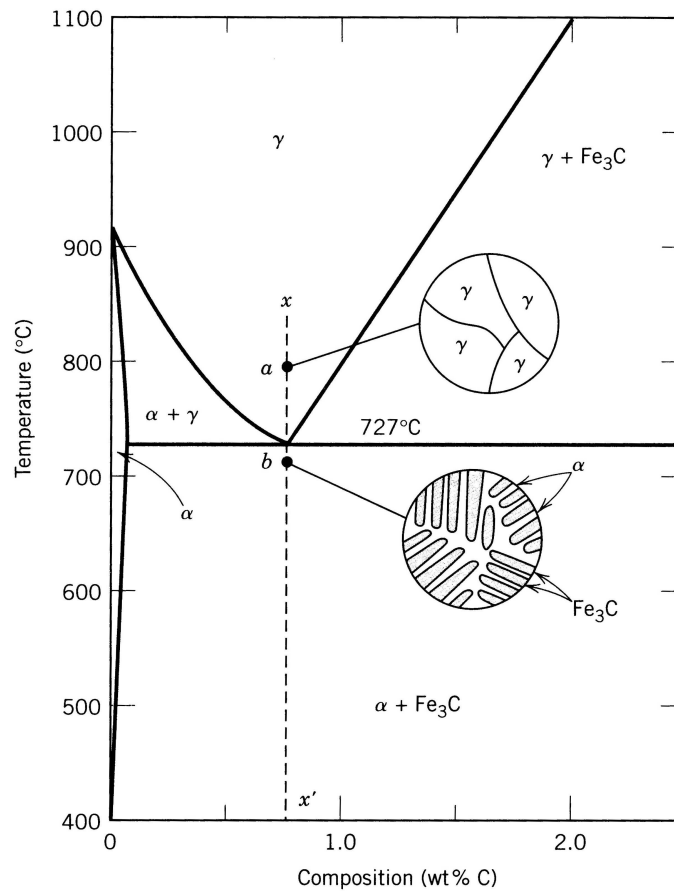


Figure 27: Phase diagram for plain carbon steels [40].

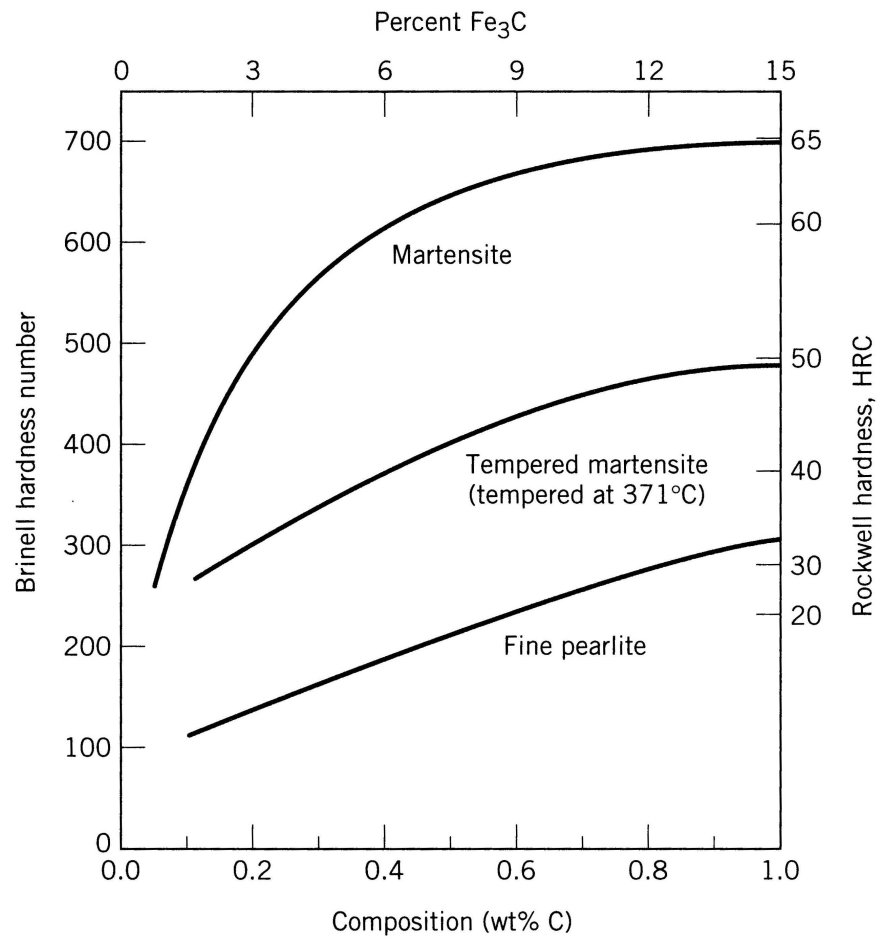


Figure 28: Hardness versus carbon concentration in plain carbon steels [40].

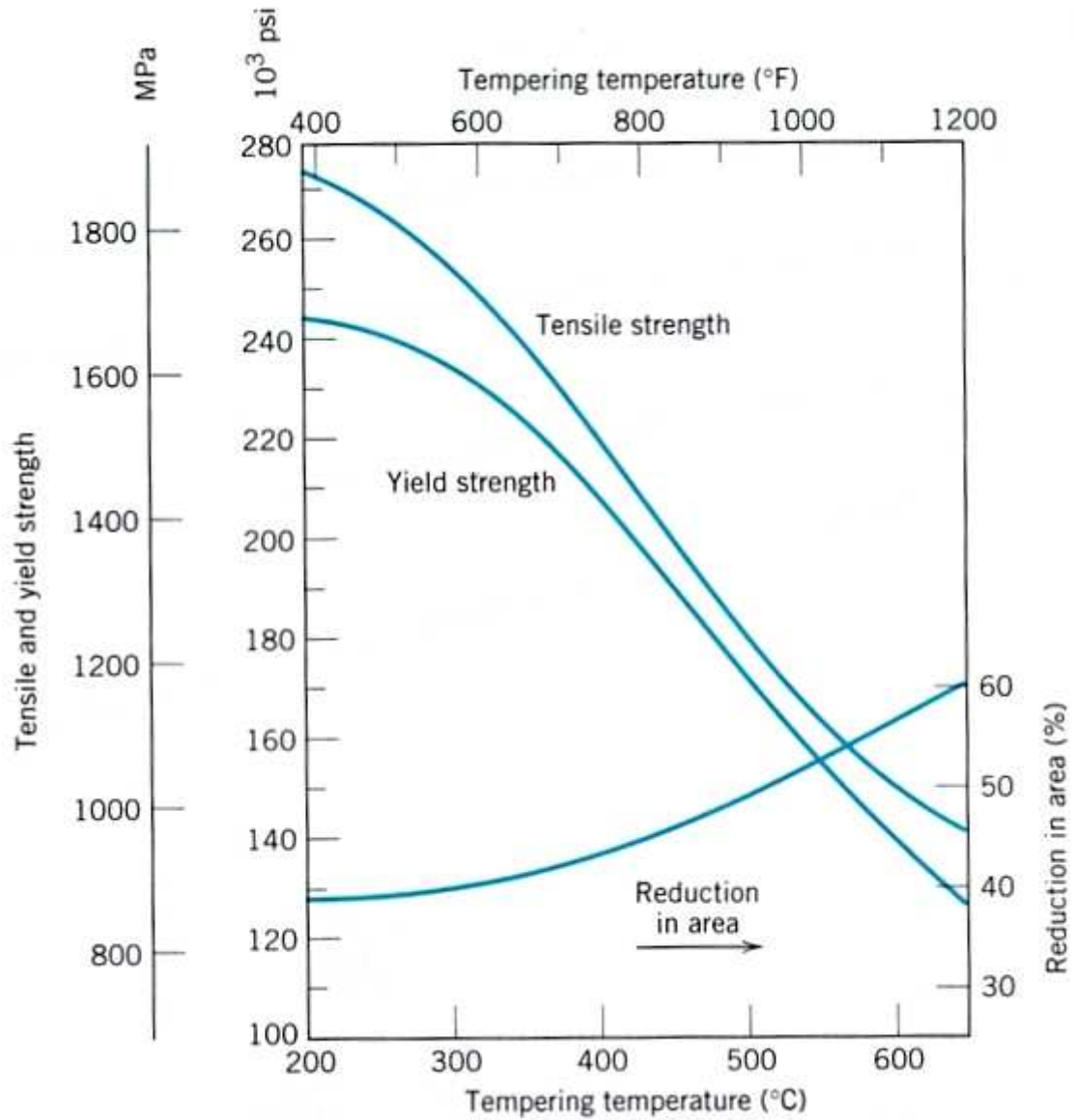


Figure 29: Tensile strength, yield strength, and reduction in area versus tempering temperature for 4340 oil quenched steel with martensitic microstructure [40].

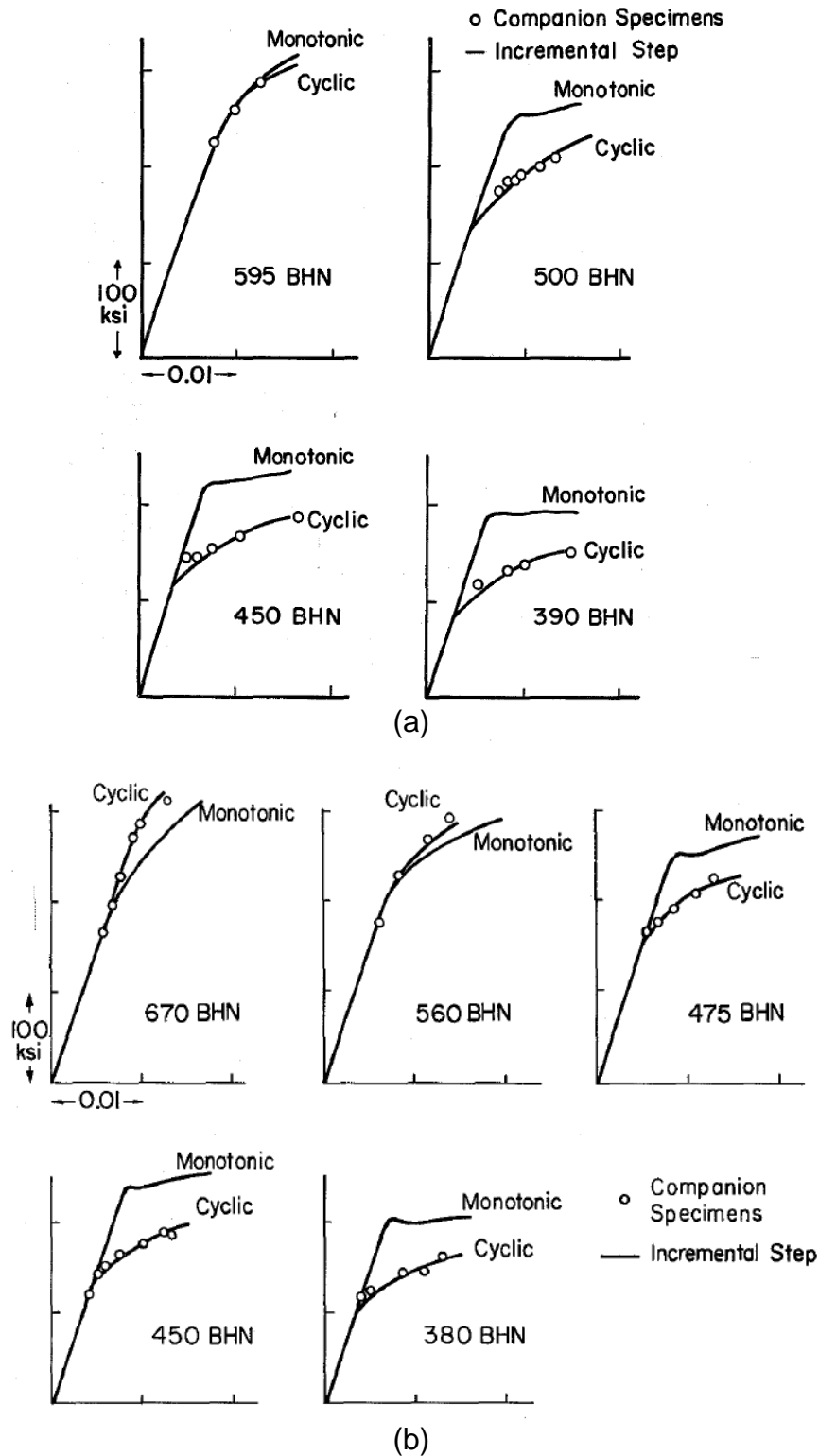


Figure 30: Monotonic and cyclic stress-strain curves for (a) SAE 1045 steel at 595 HB, 500 HB, 450 HB, and 390 HB, as well as (b) SAE 4142 steel at 670 HB, 560 HB, 475 HB, 450 HB, and 380 HB [41].

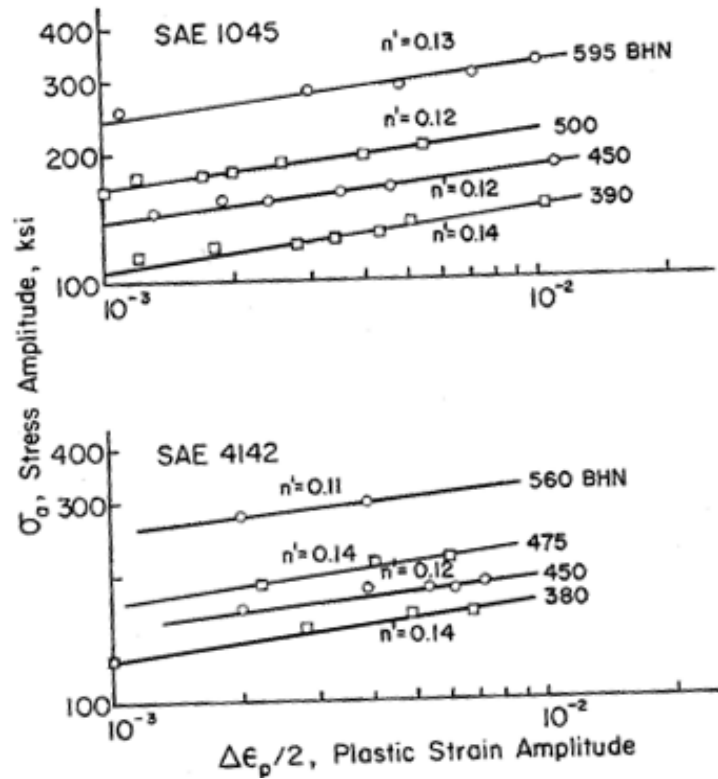


Figure 31: Stress amplitude versus plastic strain amplitude for SAE 1045 steel at 595 HB, 500 HB, 450 HB, and 390 HB, and for SAE 4142 steel at 670 HB, 560 HB, 475 HB, 450 HB, and 380 HB [41].

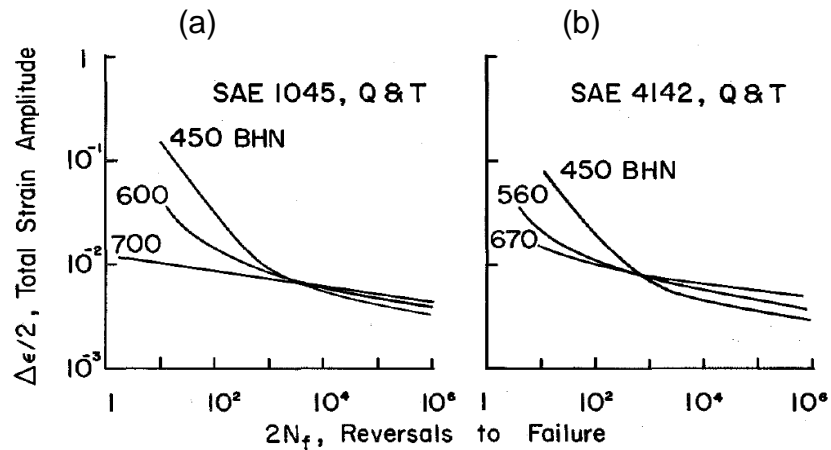
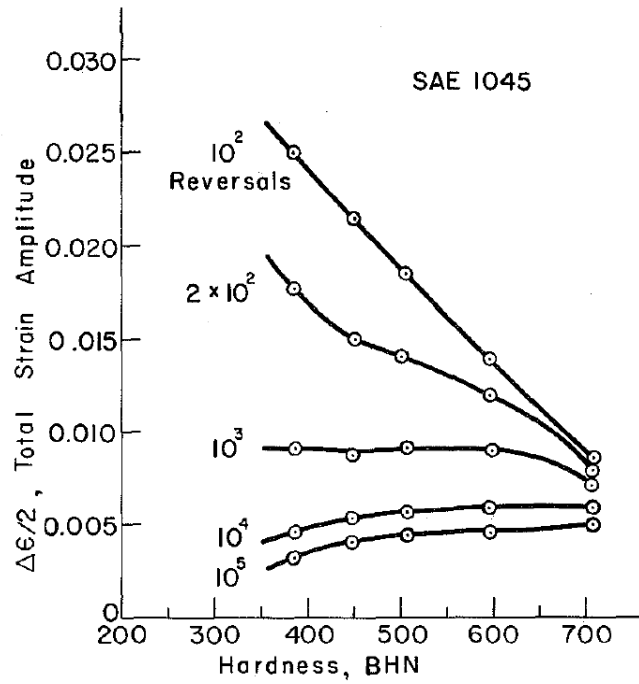
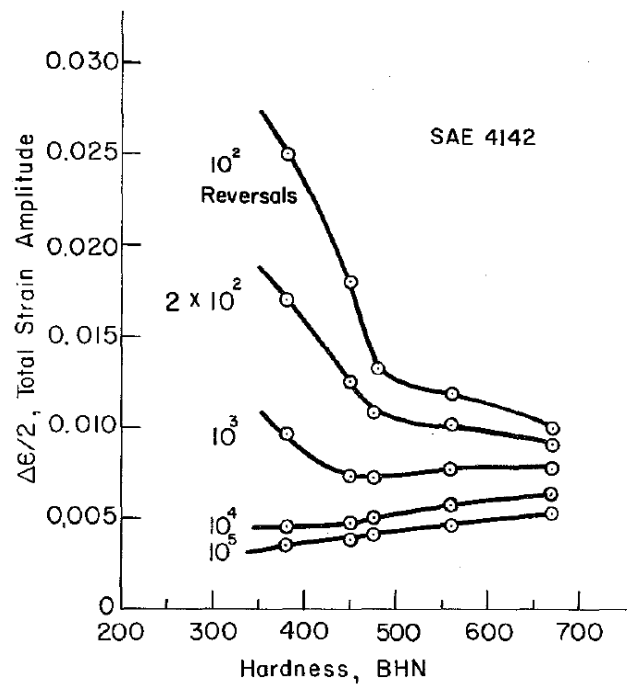


Figure 32: Total strain amplitude versus cycles to failure for strain-controlled completely-reversed fatigue testing of (a) SAE 1045 steel at 700 HB, 600 HB, and 450 HB, as well as (b) SAE 4142 steel at 670 HB, 560 HB, and 450 HB [41].



(a)



(b)

Figure 33: Total strain amplitude versus hardness for different cycles to failure for strain-controlled completely-reversed fatigue testing of (a) SAE 1045 steel, and (b) SAE 4142 steel [41].

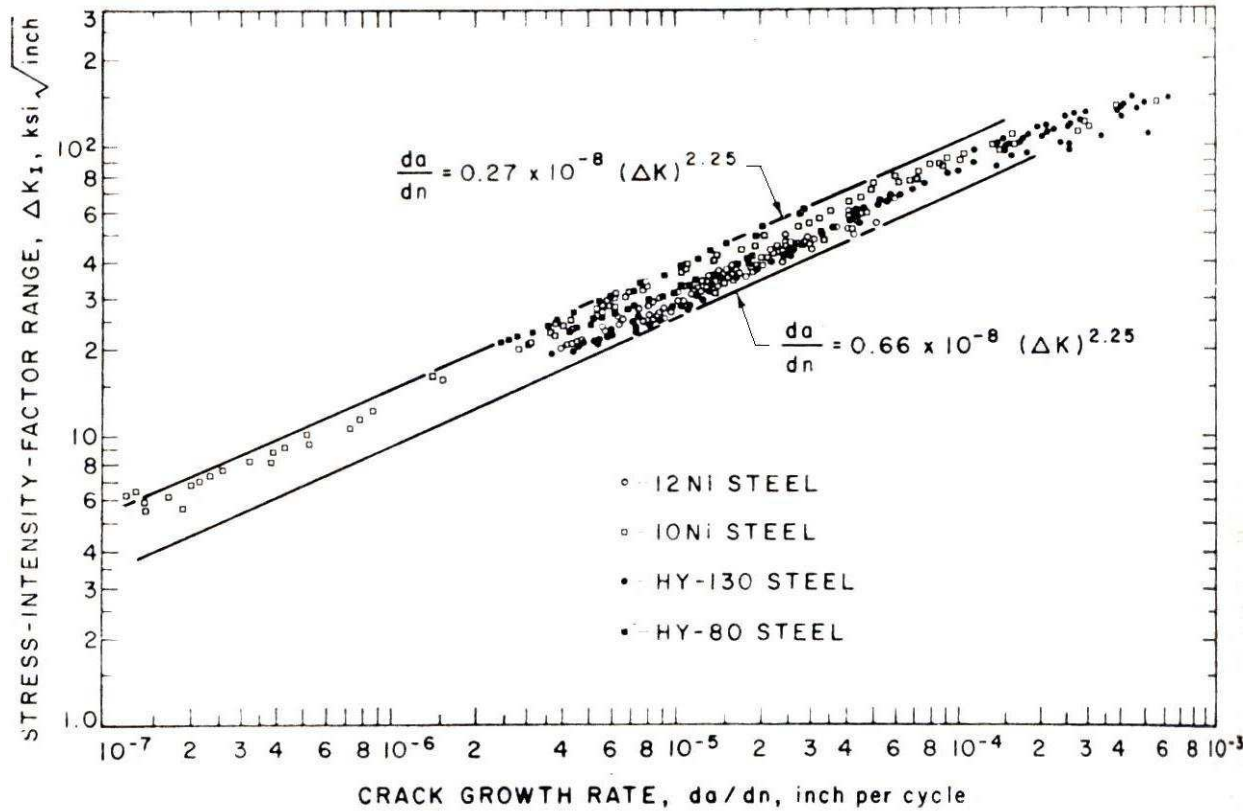


Figure 34: Plot of growth rate (da/dN) versus stress intensity factor range (ΔK) for martensitic steels having various yield and tensile strengths [42].

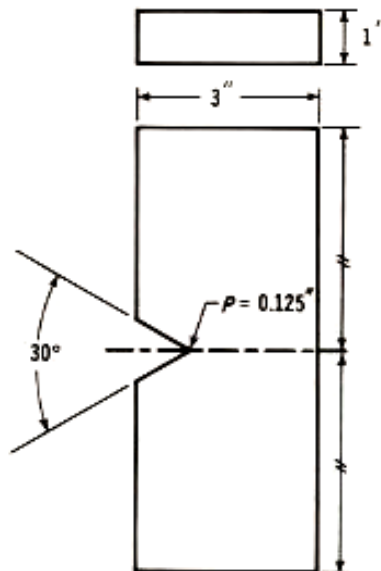


Figure 35: Specimen configuration and dimensions for a 4340 low alloy steel notched specimen used to determine the effect of decarburization on fatigue behavior in [43].

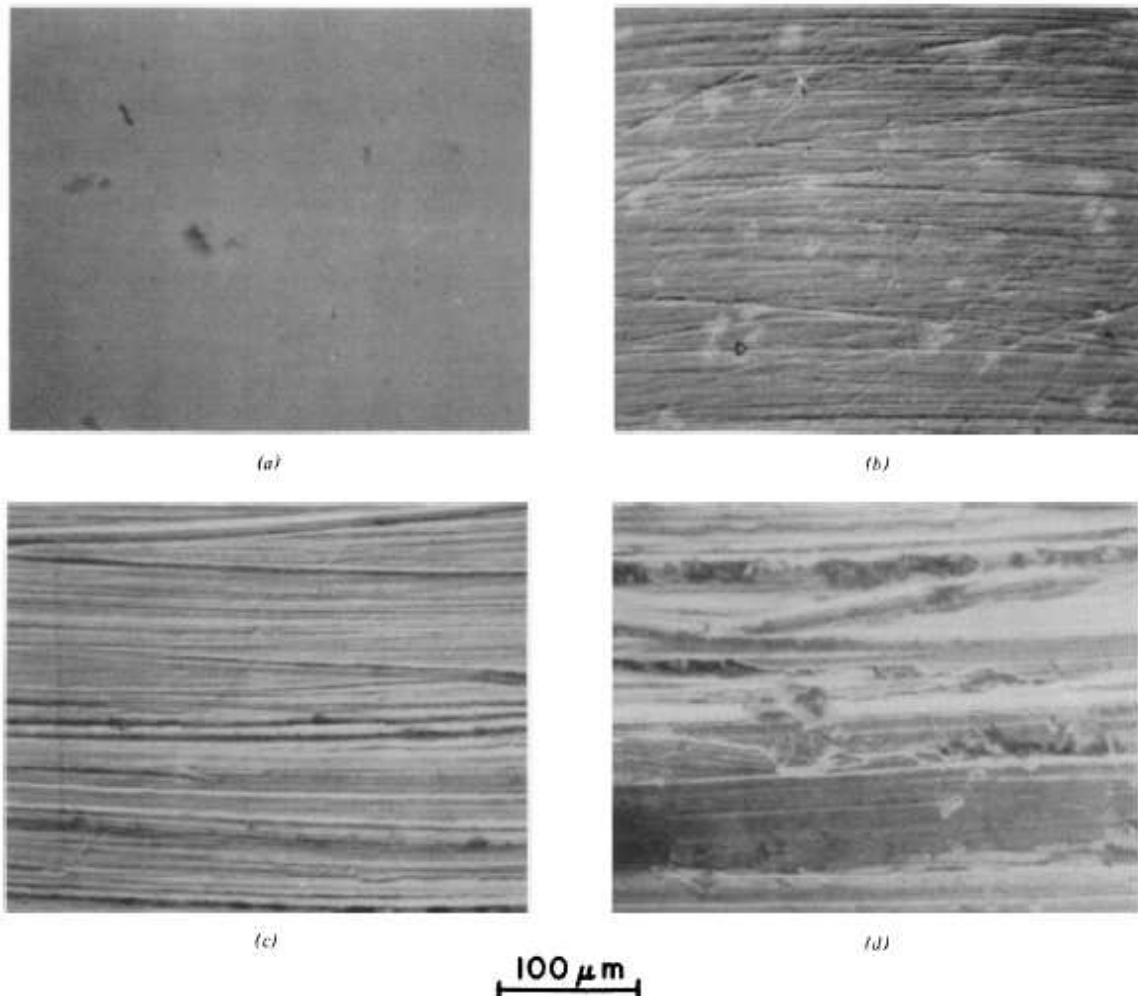


Figure 36: Magnified image of surface roughness for type 304 stainless steel having (a) ground and polished surface, and surface roughened with (b) 600 grit, (c) 240 grit, and (d) 50 grit sand paper [44].

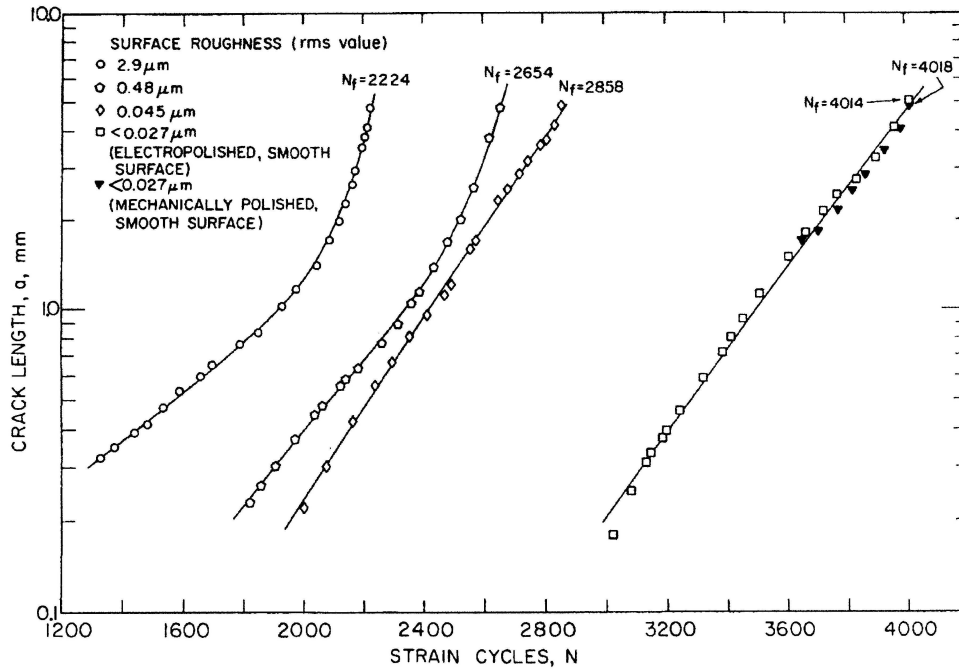


Figure 37: Crack length versus number of cycles for type 304 stainless steel specimens at four levels of surface roughness [44].

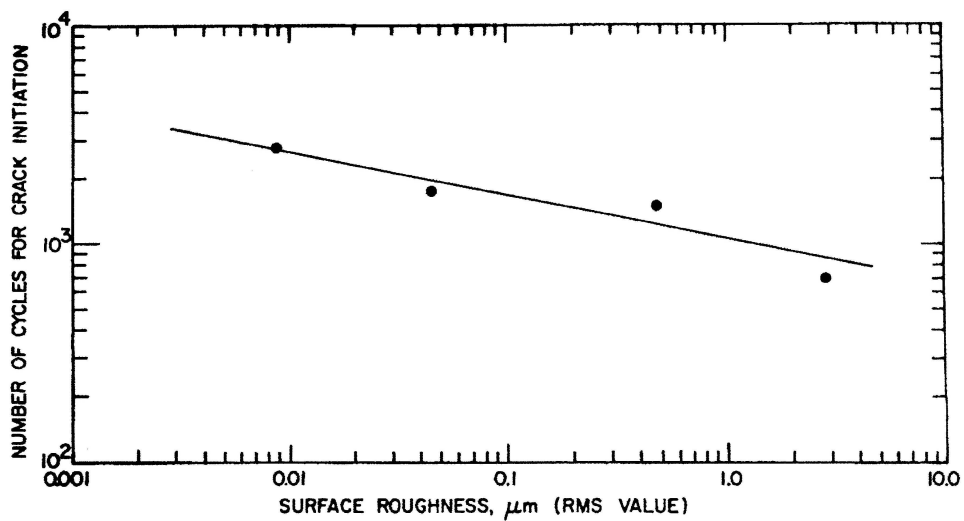


Figure 38: Crack initiation life versus surface roughness for type 304 stainless steel specimens [44].

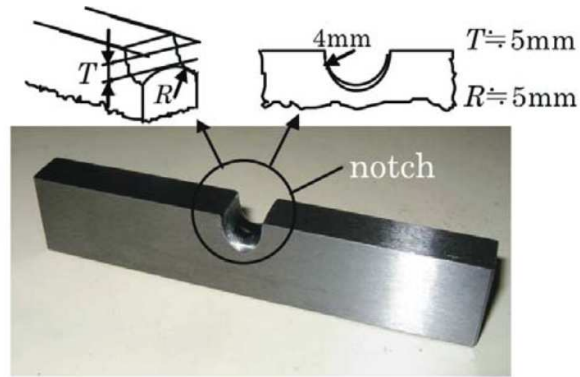


Figure 39: Notch geometry of three-point bending steel specimen with hardness between 180 HB and 230 HB used for crack growth study in [45].

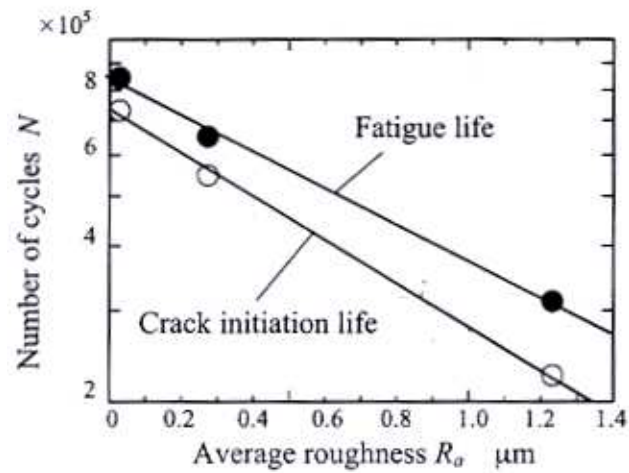


Figure 40: Number of cycles versus average roughness for three-point bending steel specimens with hardness between 180 HB and 230 HB [45].